AD-A045 108 LOUISIANA STATE UNIV BATON ROUGE COASTAL STUDIES INST F/G 8/3
RESPONSE OF COASTAL WATERS TO ATMOSPHERIC FRONTAL PASSAGE IN TH--ETC(U)
MAY 77 E DADDIO N00014-75-C-0192
UNCLASSIFIED TR-234 NL

2 OF 2
ADA
045108

END
DATE FILMED
12-78
DDC

SUPPLEMENTARY

INFORMATION

AD-A045108

ERRATA

Technical Report No. 234 (May 1977)

RESPONSE OF COASTAL WATERS TO ATMOSPHERIC FRONTAL PASSAGE IN THE MISSISSIPPI DELTA REGION

By Ernest Daddio

p. 22, line 4:
"$Q_{uv}(\omega) = -Q_{uv}(\omega)...$" should read "$Q_{uv}(\omega) = -Q_{uv}(-\omega)$"

p. 23, equation 35:
"$P_{vv}(\omega) = 2S_{vv}(\omega) = (c^2 + b^2)/2$" should read "$P_{vv}(\omega) = 2S_{vv}(\omega) = (c^2 + d^2)/2$"

AD-A045 108 LOUISIANA STATE UNIV BATON ROUGE COASTAL STUDIES INST F/G 8/3
RESPONSE OF COASTAL WATERS TO ATMOSPHERIC FRONTAL PASSAGE IN TH--ETC(U)
MAY 77 E DADDIO N00014-75-C-0192
UNCLASSIFIED TR-234 NL

1 OF 2
AD A045 108

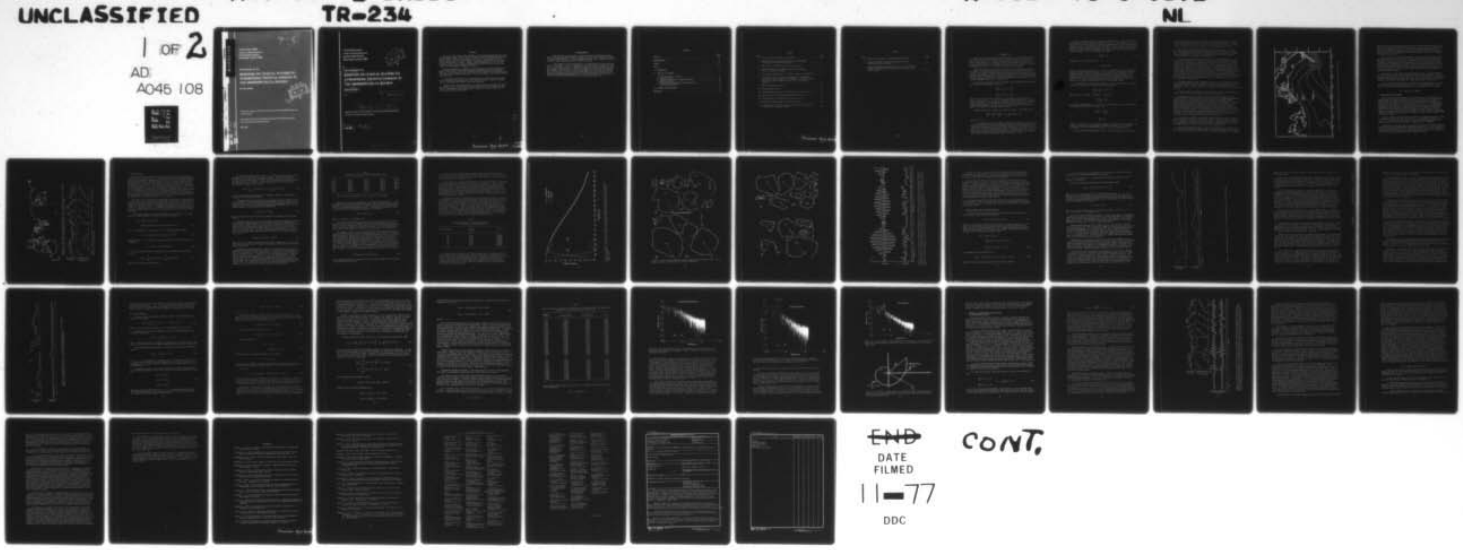

END
DATE FILMED
11-77
DDC

CONT.

Coastal Studies Institute
Center for Wetland Resources
Louisiana State University
Baton Rouge, Louisiana 70803

Technical Report No. 234

RESPONSE OF COASTAL WATERS TO ATMOSPHERIC FRONTAL PASSAGE IN THE MISSISSIPPI DELTA REGION

By Ernest Daddio

This research is supported by the Office of Naval Research under Contract N00014-75-C-0192, under Project NR 388 002.

May 1977

Coastal Studies Institute
Center for Wetland Resources
Louisiana State University
Baton Rouge, Louisiana 70803

(9) Technical Report, No. 234

(6) RESPONSE OF COASTAL WATERS TO ATMOSPHERIC FRONTAL PASSAGE IN THE MISSISSIPPI DELTA REGION

By (10) Ernest Daddio

(14) TR-234

(15) N00014-75-C-0192

(11) May 1977

(12) 46p.

ABSTRACT

Two current vector time series obtained in the Mississippi Bight exhibit clockwise polarized currents of near-inertial frequency that are closely associated with shifting winds. Because of the closeness of the local inertial period and the diurnal tidal period, it is difficult at first glance to determine the true nature of the observed rotary currents. However, complex demodulation at the inertial frequency reveals a strong signal accompanying wind shifts that are usually associated with the passage of atmospheric fronts.

Spectral analysis for clockwise and counterclockwise frequencies indicates a highly energetic peak in the inertial-diurnal frequency band for the clockwise spectrum. The rotary coefficient computed from the autospectra and quadrature spectrum of the vector components gives $C_R > 0.9$ in the vicinity of the inertial-diurnal frequency band.

A model using wind stress as a forcing function is highly effective in reproducing sinusoidal oscillations seen in the observed current. These oscillations occur in conjunction with shifts in the wind direction.

Because of the close association of the near-inertial oscillations with local wind effects, it is concluded that inertial currents are locally induced by wind stress. Furthermore, wind stress not only initiates the rotary currents but is also highly effective in destroying them.

ACKNOWLEDGMENTS

This study was conducted under a contract between the Geography Programs, Office of Naval Research, Arlington, Virginia 22217, and Coastal Studies Institute, Louisiana State University. Louisiana Offshore Oil Port, Inc., sponsored the acquisition of current and wind data at the Chevron platform.

I am indebted to the following people and organizations for their contributions to this paper: Dr. Wm. J. Wiseman, Jr., for his patient and competent supervision of my research as well as insightful suggestions and criticisms of my work; Drs. Stephen P. Murray and S. A. Hsu for very helpful and informative discussions; Ms. Mary White for her help in Fortran programming; Mrs. Gerry Dunn for drafting most of the figures; Dr. Myron Young, who developed the computer program for the binomial and Doodson-Warburg filters; U.S. Coast Guard, Grand Isle, Louisiana, for tide data; and the National Weather Service for meteorological data.

CONTENTS

FIGURES

TABLES

I. INTRODUCTION

Inertial-period oscillation of horizontal currents is a phenomenon that has been observed at a variety of depths and locations on the globe. The inertial period, T_I, is equal to $2\pi/f$, where f is the Coriolis parameter, defined as $f = 2\Omega\sin\phi$. The quantity Ω is the angular velocity of the earth's rotation and ϕ is the geographical latitude. The inertial period varies from a value of 12 hours at the poles, to 24 hours at 30° latitude, to infinity at the equator.

Under ideal conditions, inertial oscillations in a horizontal current field occur under a free-flow regime when no forces act on the fluid other than the Coriolis. The effect of Coriolis force is to deflect the motion to the right in the northern hemisphere, and therefore its only influence is in changing the flow direction and not the magnitude. Under these conditions, water flows in horizontal circular motion, clockwise in the northern hemisphere and counterclockwise in the southern hemisphere with period of rotation T_I.

The horizontal equations of motion (Neumann, 1968; Neumann and Pierson, 1966) for the case of accelerated currents are

$$\frac{du}{dt} = fv - F_x - \alpha \frac{\partial P}{\partial x}$$

$$\frac{dv}{dt} = -fu - F_y - \alpha \frac{\partial P}{\partial y} \qquad (1)$$

where u is the speed in the x direction, v is the speed in the y direction, $d/dt = \partial/\partial t + u\ \partial/\partial x + v\ \partial/\partial y$ is the so-called "material derivative," f is the Coriolis parameter, F_x and F_y are the frictional forces along the x and y directions, respectively, α is the specific volume, and P is the pressure. If the Guldberg-Mohn assumption is used to describe the frictional forces, then $F_x = ku$ and $F_y = kv$, where k is a proportionality constant.

Multiplying the first equation by u and the second by v and adding yields

$$u \frac{du}{dt} + v \frac{dv}{dt} = \frac{1}{2} \frac{dc^2}{dt} = -\alpha \left(u \frac{\partial P}{\partial x} + v \frac{\partial P}{\partial y}\right) - kc^2 \qquad (2)$$

where $c^2 = u^2 + v^2$.

For a homogeneous ocean, the pressure gradients in equation 2 can result only from a slope of the sea surface. Although the slope of the sea surface can be a significant driving force in coastal regions, the site of this study seems to be sufficiently far from the nearest coast (about 25 km) that slope effects are negligible, at least in the diurnal frequency band. The model used in this report assumes that no pressure effects were present, yet it gives excellent correspondence between observed and modeled currents (see Section II-E).

On the other hand, sea surface slopes represent potential energy that may later be converted to kinetic energy of the inertial currents. For example, if a wind stress that sets up and maintains a slope is suddenly removed, the slope may rapidly disappear and the stored energy will be converted to current motion. Such current motion is acted upon mainly by friction and Coriolis force. The result is a damped current rotating at inertial frequency. Therefore, if we require the horizontal pressure gradient to go to zero, equation 2 becomes

$$\frac{1}{c}\frac{dc}{dt} = -k \ . \tag{3}$$

Integration of this equation yields

$$c = c_o \exp(-kt) \tag{4}$$

where c_o is the current speed at $t = 0$. For $k = 0$, equation 3 is the equation for a pure frictionless inertial current. For $k \neq 0$, equation 3 represents a damped inertial current. Equation 4 indicates that decay of current magnitude is an exponential function of k. The value of k can vary from place to place in the ocean; typical values of 10^{-6} to 10^{-7} sec^{-1} have been reported by Defant; 0.7×10^{-5} sec^{-1}, by Gustafson and Kullenberg for the Baltic Sea; and 3×10^{-6} sec^{-1}, by Neumann for the upper thousand meters of the ocean (Neumann, 1968).

If we multiply the first part of equation 1 by v and the second by u and then subtract, we obtain, for no horizontal pressure gradient,

$$v\frac{du}{dt} - u\frac{dv}{dt} = f(u^2 + v^2) \ . \tag{5}$$

Now, $d/dt\,(u/v) = (vdu/dt - udv/dt)/v^2$. Therefore,

$$v^2 \frac{d}{dt}\left(\frac{u}{v}\right) = \frac{f}{c^2} \ . \tag{6}$$

In Cartesian coordinates $u/v = \cot\beta$ and $v^2 = c^2\sin^2\beta$, where β is the angle between the x-axis and the current direction. Thus,

$$\frac{d}{dt}\cot\beta = \frac{f}{\sin^2\beta}$$

or

$$\frac{d\beta}{dt} = -f \ . \tag{7}$$

Equation 7 states that the time rate of change of the direction of an inertial current is a constant that is the negative Coriolis parameter. In the northern hemisphere $\phi > 0$, $f > 0$, and therefore $d\beta/dt < 0$, i.e., clockwise motion.

The present investigation makes use of a 32-day (28 January to 28 February

1974) moored current meter record obtained in the Mississippi Bight by members of the Coastal Studies Institute as part of the Louisiana Offshore Oil Port (LOOP) project (Wiseman et al., 1976). A second record, comprising 39 days, is also discussed, but analysis was limited because of lack of meteorological data.

The current meter was moored south of Grand Isle, Louisiana, at latitude 28°55'N, longitude 89°47'W, and 6.4 meters below the surface in water 33 meters deep. Wind data was obtained from an anemometer placed on a Chevron rig located about 15 km northwest of the site of the current meter at latitude 28°01'N, longitude 90°06'W. (See Figure 1 for locations.)

It is the purpose of this study to show that inertial-period motions in the study area are excited by strong winds, in particular those winds that accompany atmospheric frontal passage. The major difficulty in quantitatively discerning these motions from others arises from the fact that the inertial period at the latitude of the study site is 24.76 hours, which corresponds approximately to the diurnal tidal period. This problem has plagued a number of researchers who have worked at latitudes near 30°. Webster (1968), in a comprehensive review, listed 24 significant studies that involve inertial-period oscillations spanning the years 1931 to 1966. He noted that in the older literature it is often difficult to determine whether what the researchers reported were indeed inertial motions. On the other hand, certain investigators may have been reluctant to report ambiguous results as inertial motions, and consequently their findings may not be part of the literature on the subject.

According to Webster (1968), important early work on the subject was done by Ekman and Helland-Hansen, who in 1930 made a series of current measurements near latitude 30° north. They found diurnal fluctuations in the signal that were interpreted as tidal motion. Ekman later concluded that these were in fact inertial motions.

In later studies, Stommel (1954) reported inertial motions near Bermuda, and Swallow (1957) found this phenomenon in the eastern Atlantic.

Investigations near latitude 30° north during the early 1960s seemed to indicate that inertial-period motions were the result of a resonance phenomenon of the diurnal tide at the diurnal inertial latitude. Knauss (1962) tracked Swallow floats at several depths in the North Pacific near latitude 28° north and noticed a diurnal clockwise rotary motion. Because the recorded speeds were several times greater than the expected tidal currents in the open ocean, he reasoned that they were due to internal waves of inertial period. Knauss considered the concept of the earth's latitude bands acting as tuned circuits, each tuned to its inertial period. In the vicinity of latitudes 29° and 75°, the ocean is tuned to the diurnal and semidiurnal components, respectively, of the tide-producing forces. Strong inertial motions, then, should be found only at those latitudes in tune with generating forces, and nowhere else.

A study by Reid (1962) at latitude 30° north in the Pacific added support to Knauss' findings. Reid found that surface currents having a period of rotation of 24 hours were in phase with the diurnal tide. He further noted an oscillation of the temperature structure of 12.4-hour period; he suggested that the oscillation might represent internal waves of lunar semidiurnal period.

Observations by Hunkins (1967) of inertial oscillations of ice island T-3 in the Arctic Ocean tended to repudiate Knauss' and Reid's findings. Hunkins noted that "inertial oscillations of floating ice are generated in response to changing

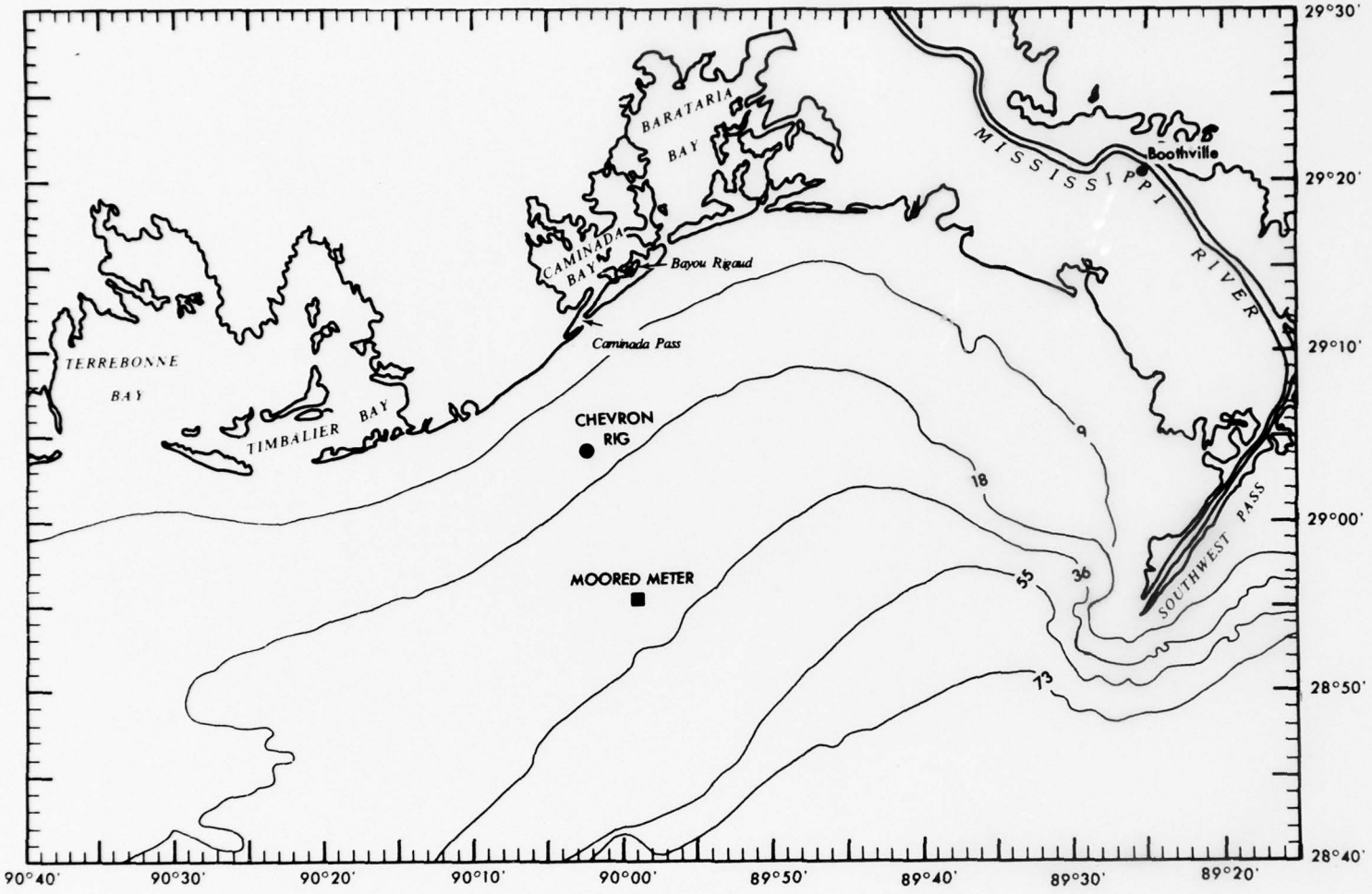

Figure 1. Study region and locations of instruments. Contours show depth in meters.

wind stress and would presumably involve only the ice and the upper layers of the ocean. Their amplitude would reflect changes in the wind, and their phase would be expected to change with each wind system." His observed oscillations were of a shorter period than the semidiurnal tidal period, changed amplitude in response to the wind, arbitrarily changed phase, and were restricted to the ice and, possibly, the uppermost water layers.

A long record of currents was obtained by Bernstein (1972) from current meters set below ice island T-3 in the Arctic Ocean. He identified inertial motions in the mixed layer below the ice despite contamination of the current record by the semidiurnal tidal period, which was nearly the same as the local inertial period. The mechanism of generation in this case was the stress produced by the ice as it moved over the well-mixed surface layer. Among the evidence he cited was the fact that the currents were much too strong to be caused solely by the tide and that their spectral peak was centered on a frequency closer to the inertial than to the semidiurnal tidal frequency.

Among the most recent work on inertial motions is that of Pollard (1970) and Pollard and Millard (1970), who were able to model inertial oscillations of near-surface currents induced by wind stress alone. They were successful in reproducing observed oscillatory motions with a model that assumes a surface wind stress instantaneously and uniformly distributed as a body force through the mixed layer.

Perkins (1970) observed inertial oscillations in the Mediterranean. He separated the inertial motions from the current record and determined their rate of decay by the method of complex demodulation to be described later in this paper.

II. ANALYSIS OF CURRENTS

A. Progressive Vector Diagram

When the February 1974 observed currents are plotted as a progressive vector diagram, some interesting features of the current field emerge. The progressive vector diagram is simply the observed current vectors plotted end to end. It describes the path taken by a particle under the influence of a horizontally uniform current field identical to the currents at the study site. In examining the progressive vector diagram, it should be remembered that it shows displacements caused only by currents at the measuring site. If, for example, a drogue were placed at the study site and tracked for a period of time, it would encounter a variety of current regimes and its displacement would reflect particle displacement under the influence of those regimes. In general, its path would be different from that shown in Figure 2.

Figure 2 suggests rotational motion superposed on translational motion. Especially interesting are the loops in the plot for the approximate periods 4 to 7, 9 to 15, 17 to 20, and 25 to 27 February. This is precisely the motion to be expected when the observed current has a significant rotary component.

Examination of the wind record at the Chevron rig (Fig. 3) indicates that the observed rotation is associated with significant wind events. It will be shown in this paper that the periods indicated above are examples of inertial oscillations of the surface layer of the ocean. Other examples also exist in the record but are not as obvious in the progressive vector diagram as the above.

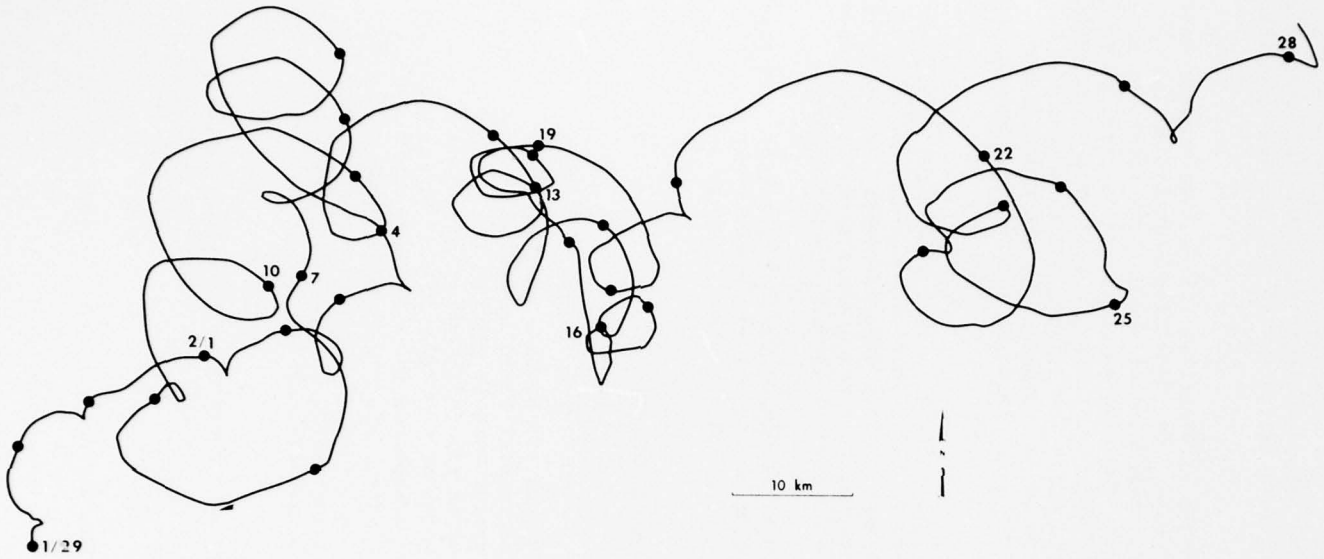

Figure 2. Progressive vector diagram for current record beginning 29 January and ending 28 February 1974. Each dot indicates 0000 hour on the indicated date.

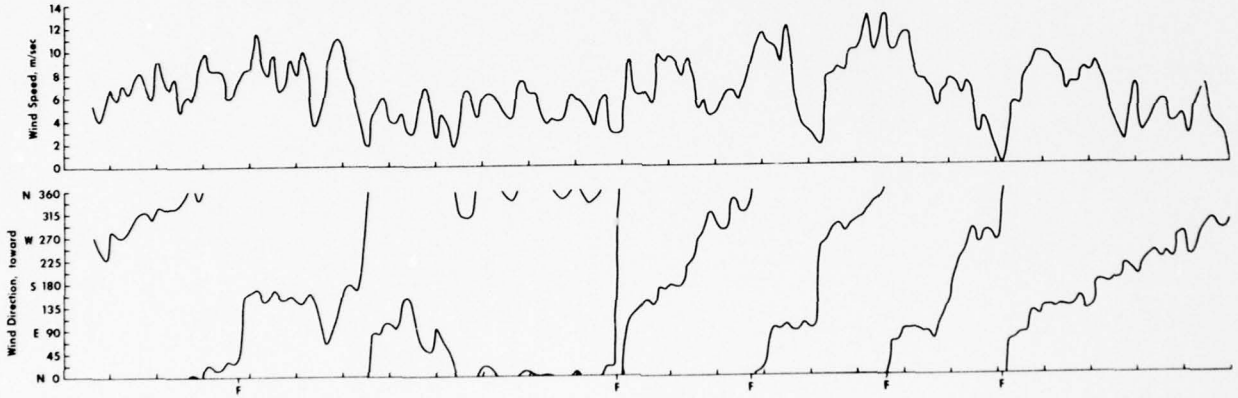

Figure 3. Wind record at Chevron rig for 4-28 February 1974. F indicates approximate times of frontal passage.

B. Data Filtering

Extracting tidal currents from a current record can present some annoying difficulties. The problem is one of selecting a filter or set of filters that will give the truest possible reproduction of a signal at the desired frequencies while suppressing the signal at unwanted frequencies, i.e., selecting filters having a desirable frequency response. The frequency response of a filter is the ratio of the amplitude of a wave of a given frequency in the time series after filtering to the original amplitude. It can be determined by examining the effect of the filter on a unit-amplitude sinusoidal wave of frequency σ (Holloway, 1958). Such a wave may be visualized as a unit vector in the complex plane rotating at angular velocity $2\Pi\sigma$. After application of the filter, the modified wave may be represented by a new vector having the same angular velocity as the original but different magnitude and phase angle. The frequency response of the filter is then simply the ratio of the magnitude of the modified vector to the unit vector.

The filter or, more precisely, the filtering function is a mathematical operator that consists of a series of fractional values called weights. These weights determine the relative contribution of each observation in the time series to the estimate of the filtered value. The weights are convolved with the time series to perform the filtering operation. For example, the Hamming filtering function, consisting of weights 1/4, 1/2, 1/4, is symmetric and replaces a time series observation with an average obtained from half its value plus one-fourth of the two adjacent values.

The frequency response of a filtering function, $w(t)$, is given by the magnitude of its inverse Fourier transform, $R(\sigma)$, which is defined as

$$R(\sigma) = \int_{-\infty}^{\infty} w(t) \exp i(2\Pi\sigma t)\, dt$$

$$= \int_{-\infty}^{\infty} w(t) \cos(2\Pi\sigma t)\, dt + i\int_{-\infty}^{\infty} w(t) \sin(2\Pi\sigma t)\, dt \qquad (8)$$

where σ is frequency, t is time, and $i = \sqrt{-1}$. Taking the absolute value,

$$| R(\sigma) | = \left\{[\mathrm{Re}(R(\sigma))]^2 + [\mathrm{Im}(R(\sigma))]^2\right\}^{1/2} \qquad (9)$$

The phase shift, ϕ, at a particular frequency produced by the filtering process is given by

$$\phi = \arctan [\mathrm{Im}(R(\sigma))/\mathrm{Re}(R(\sigma))] \,. \qquad (10)$$

If the filtering function is composed of discrete weights, then equation 8 becomes

$$R(\sigma) = \sum_{k+-n}^{m} w_k \cos(2\Pi\sigma k) + i \sum_{k=-n}^{m} w_k \sin(2\Pi\sigma k) \qquad (11)$$

where σ is in cycles per data interval.

An important requirement in the choice of a filter is that it does not shift the phase of the record at any particular frequency. This is accomplished by choosing a set of weights that are symmetrical about some central weight, w_o, i.e., $w_{-j} = w_j$, where j is an integer. In this case, the imaginary term, the sine term in equations 8 and 11, is zero, and, from equation 10, $\phi = 0$. The frequency response for the discrete case is then

$$R(\sigma) = \sum_{k=-n}^{n} w_k \cos(2\Pi\sigma k) = w_o + 2 \sum_{k=1}^{n} w_k \cos(2\Pi\sigma k) \qquad (12)$$

for the filtering function having (2n + 1) weights. Equation 12 describes the response of a filter with zero phase.

A high-pass filter may be constructed very simply by using a low-pass filter. If a time series is first low-passed and the resulting values are then subtracted from the original series, the new series produced is a high-passed version of the original series, that is, one containing high-frequency components only. The frequency response of this process may be represented by

$$R(\sigma)_{O-LP} = 1 - R(\sigma)_{LP} \qquad (13)$$

where the subscripts 0 and LP denote the original and low-passed series, respectively.

Similarly, a band pass of a time series may be obtained by applying two filters with different frequency response to the original data and then subtracting one filtered series from the other. The two filters are chosen according to which frequencies are to be suppressed. Application of one filter is used to obtain a record with only low and intermediate frequencies. The second filter is used to pass only low frequencies. The result of subtracting the second series from the first is a band pass, which may be expressed in terms of the frequency response of the filters as

$$R(\sigma)_{LP1-LP2} = R(\sigma)_{LP1} - R(\sigma)_{LP2} \qquad (14)$$

where LP1 and LP2 represent low-pass filters 1 and 2, respectively. This process will remove both high- and low-frequency components and will yield values at intermediate frequencies.

The problem of extracting tidal currents from a current time series is one of appropriately band-pass filtering that series. An effective and surprisingly simple filter for analysis of tides, which was used in this study, was developed by Doodson and Warburg (1941). The weights of the Doodson-Warburg filter, which are used to multiply a time series with Δt = 1 hour, are shown in Table 1. These weights, which Doodson and Warburg call "multipliers for mean sea level," were derived empirically by combining several simple filters that discriminate against the principal tidal constituents and higher frequencies (Doodson and Warburg, 1941; Groves, 1955). The Doodson-Warburg filter has the desirable property of being symmetric and therefore does not change the phase of the time series.

Table 1
Numerators of Weights of the Doodson-Warburg Filter

(1) 1	(9) 1	(17) 1	(25) 0	(33) 0
(2) 0	(10) 0	(18) 1	(26) 1	(34) 1
(3) 1	(11) 2	(19) 2	(27) 1	(35) 0
(4) 0	(12) 0	(20) 0	(28) 0	(36) 0
(5) 0	(13) 1	(21) 2	(29) 2	(37) 1
(6) 1	(14) 1	(22) 1	(30) 0	(38) 0
(7) 0	(15) 0	(23) 1	(31) 1	(39) 1
(8) 1	(16) 2	(24) 2	(32) 1	

NOTE: Each value is divided by 30 to obtain the set of weights.

Another filter used in this analysis is the 31-point binomial filter. It also is a symmetrical filter whose weights are proportional to the coefficients of the expansion of the binomial form $(p + q)^n$, where n is the number of desired weights less 1 (n = 30 in this case)(Holloway, 1958). In general, the frequency response of a binomial filter as calculated from equation 8 is given by

$$R(\sigma) = \cos^n (\Pi\sigma\Delta t) \tag{15}$$

where Δt = 1/3 hour in the present case.

Recall that for increasing n, the envelope of the coefficients of the expansion of $(p + q)^n$ approaches a Gaussian curve. In both filters the sum of the weights is unity. This property of the two filters is particularly important inasmuch as each weight expresses in what proportion each of a set of observations is to be counted. Each weight is, therefore, a fractional part of a sum that is 1.

The original current record was decomposed into vector components and filtered using the binomial filter in order to remove the high frequencies. The original values were also low passed with the Doodson-Warburg filter to remove the principal tidal constituents. Because the current values were available at intervals of 1/3 hour and the Doodson-Warburg filter requires a 1-hour interval, the filter was first applied at 1-hour intervals beginning at t_o = 0 hour. It was then time shifted by 1/3 hour and applied at 1-hour intervals beginning with starting time t_o = 1/3 hour and again with t_o = 2/3 hour. The result is a filtered time series with Δt = 1/3 hour. The output of the Doodson-Warburg filter was then subtracted from the output of the binomial filter to obtain the vector components of the tidal currents. In terms of the frequency response, the process may be expressed as

$$R(\sigma)_{BD\text{-}PASS} = R(\sigma)_{BN} - R(\sigma)_{DW} \tag{16}$$

where BD-PASS represents the band-pass process, BN is the binomial filter, and DW is the Doodson-Warburg filter.

Figure 4 is a plot of the frequency response functions of the filters discussed. Notice that the 31-point binomial filter eliminates all but about 10 percent of the energy at 0.35 CPH, yet it preserves about 90 percent of the semidiurnal tide and nearly all of the diurnal tide.

On the other hand, the Doodson-Warburg filter is highly effective in eliminating the lower frequencies, specifically the diurnal and semidiurnal. Table 2, adapted from Groves (1955), gives the frequency response of the filter for the principal tidal constituents. The high-pass filter formed from the Doodson-Warburg filter, therefore, preserves almost completely those motions associated with tidal forcing. The band-pass signal found using the binomial and Doodson-Warburg filters contains about 97 percent of the current magnitude near the diurnal period, 90 percent near the semidiurnal, and 65 percent near the quarter-diurnal. Energy at periods greater than 2 days is greatly reduced.

A band-passed version of the February data was obtained and plotted in Figure 5 as hodographs for each 24-hour period beginning at 0000 hour and ending at 2300 hour of each day. The hodograph represents the path traced by the tip of the tidal current vector over a 24-hour period. If we assume that large tidal range (Fig. 6) must produce strong tidal currents and small tidal range must produce weak tidal currents (Sverdrup et al., 1942), the relative sizes of the hodographs are rather surprising. For example, 31 January through 3 February is a period of rather large tidal range, but the hodographs indicate generally weak currents. From 8 through 12 February is a period of equatorial tides (minimum tidal range), but the hodographs are the largest of the study. Consider also the hodographs of 25 and 26 February, which show strong tidal currents for a period of equatorial tides.

Table 2

Frequency Response of Doodson-Warburg Filter
to the Principal Tidal Constituents

Tidal Constituent	Period (Hours)	$R(\sigma)$
M_2	12.42	-0.00058
S_2	12.00	0.00000
N_2	12.66	0.00171
K_2	11.97	0.00033
K_1	23.93	0.00015
O_1	25.82	0.00299
P_1	24.07	-0.00013

It appears that some process other than astronomical tidal forcing is putting energy into the tidal frequency band. The wind record (Fig. 3) obtained at the Chevron platform and the Weather Bureau record for Boothville, Louisiana (not shown) reveal a very strong correlation between times of shifting wind direction and increased wind speed (usually associated with atmospheric fronts) and large well-defined "tidal ellipses." At other times the hodographs have a generally ragged and somewhat confused appearance.

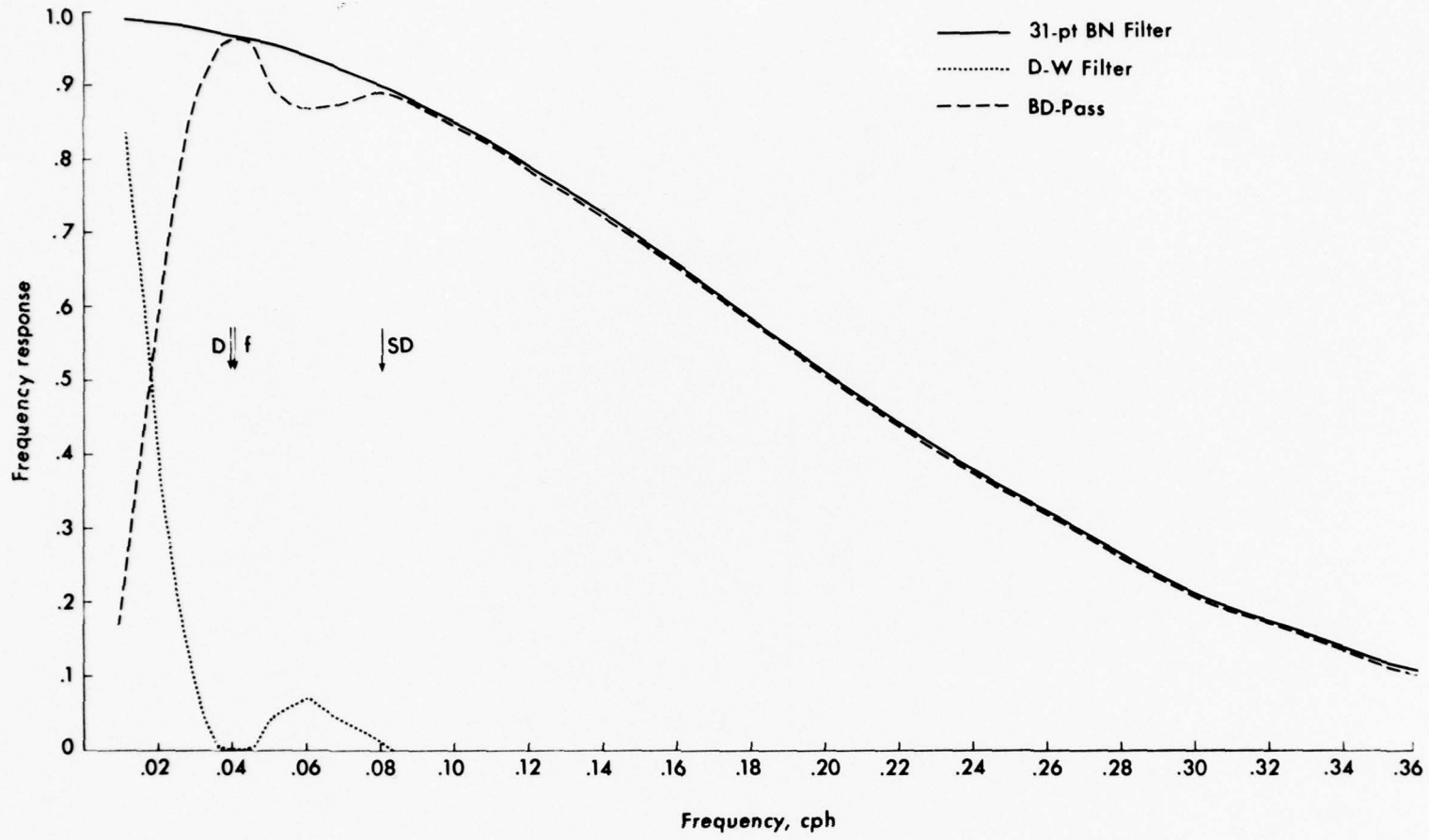

Figure 4. Frequency response of binomial filter (BN), Doodson-Warburg filter (DW), and band-pass process (BD-Pass). D, f, and SD represent the diurnal, inertial, and semidiurnal frequencies, respectively.

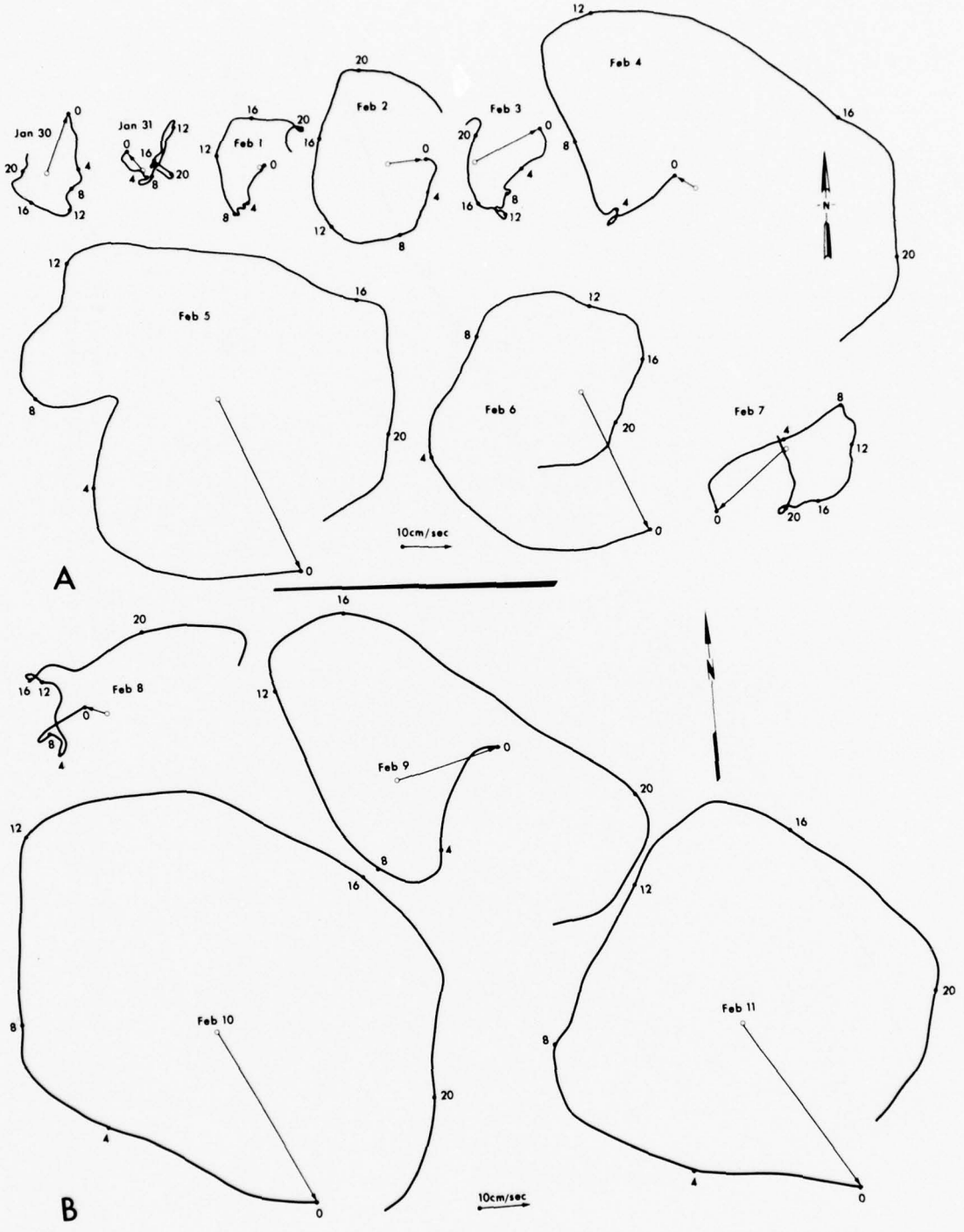

Figure 5. Daily current hodographs for 30 January through 26 February 1974. Arrows indicate magnitude and direction of current at 0000 hour.

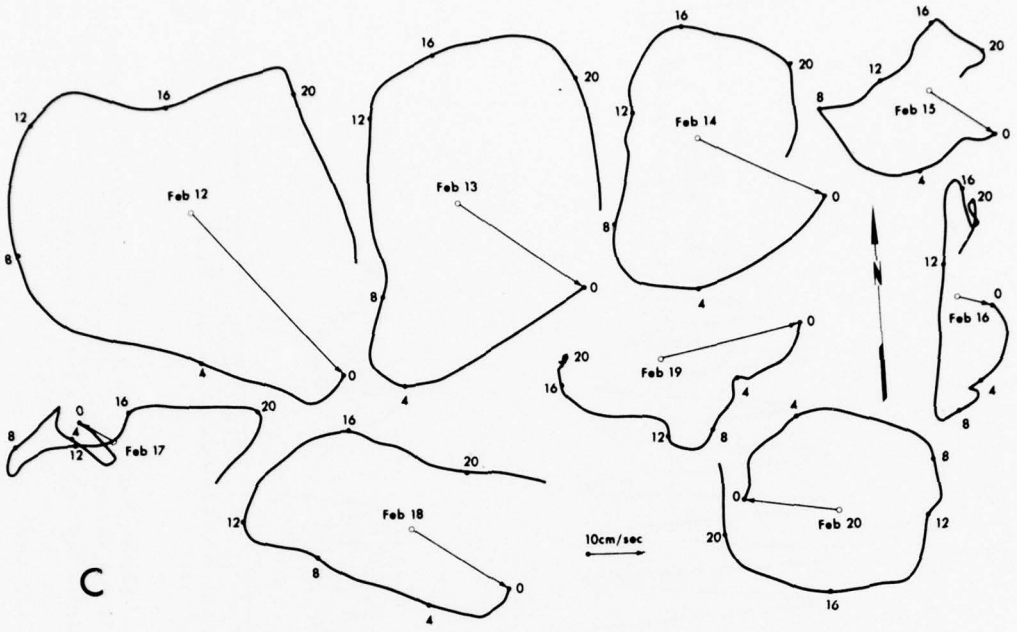
Feb 12
Feb 13
Feb 14
Feb 15
Feb 16
Feb 17
Feb 18
Feb 19
Feb 20
10cm/sec
N
C

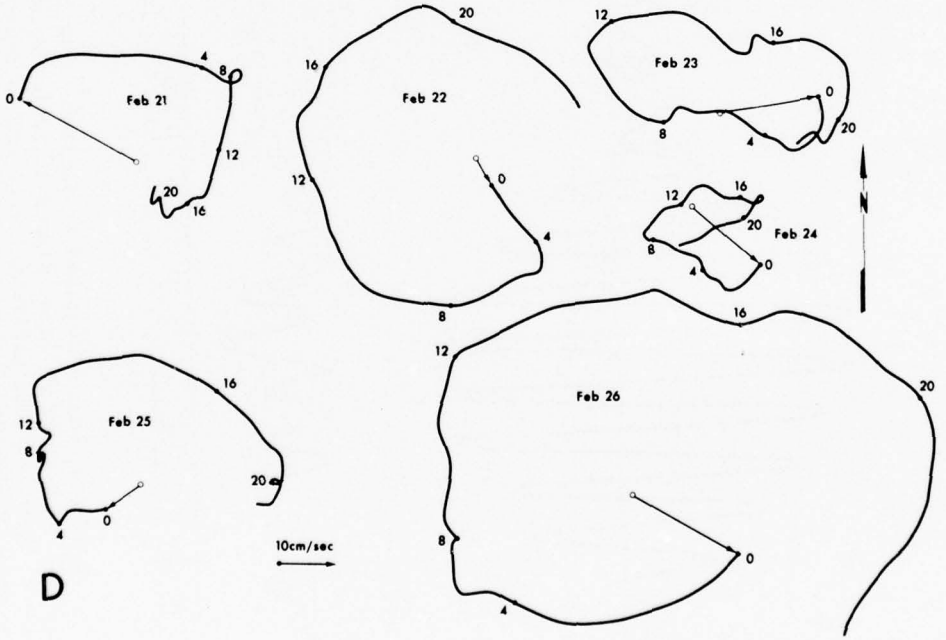
Feb 21
Feb 22
Feb 23
Feb 24
Feb 25
Feb 26
10cm/sec
N
D

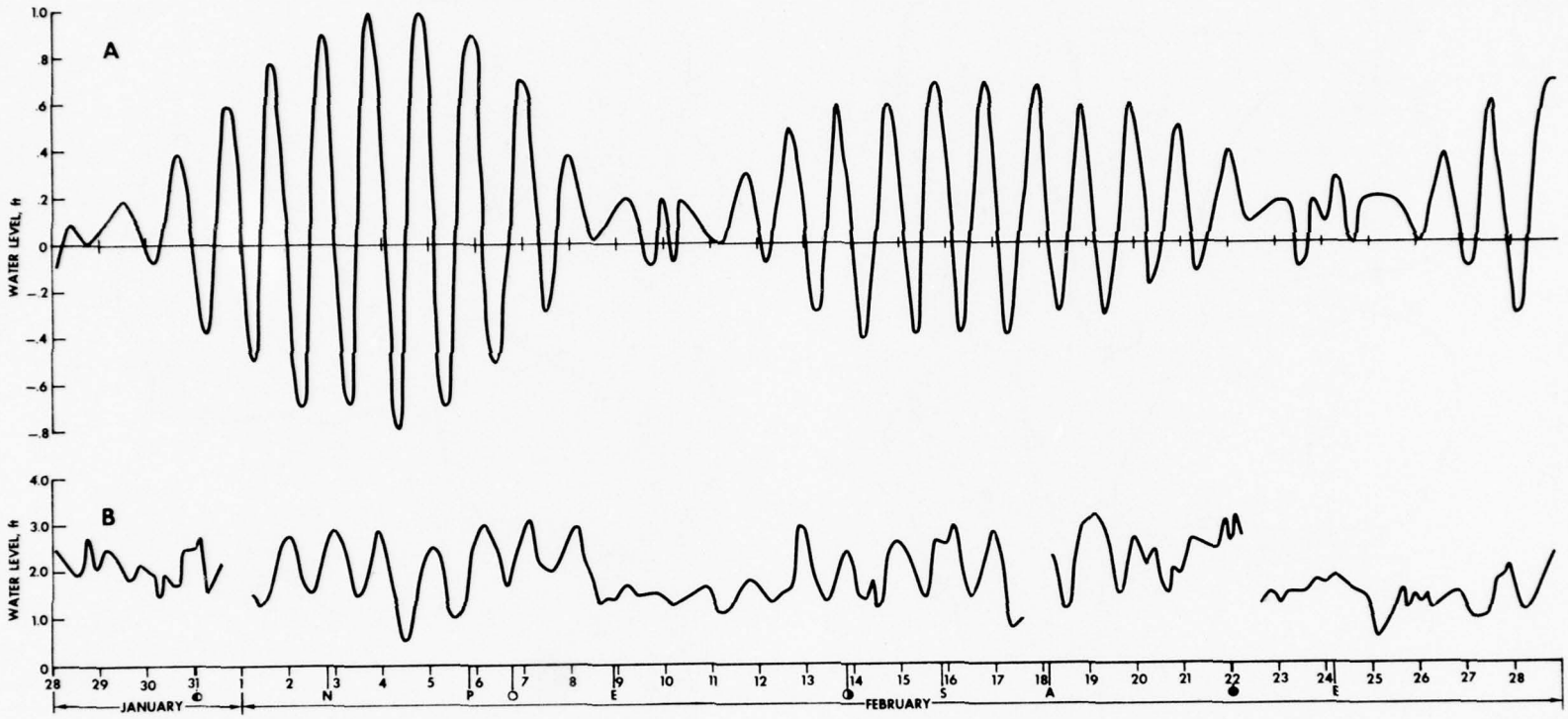

Figure 6. A. Predicted tidal elevations at Caminada Pass from National Ocean Survey tables, Department of Commerce. B. Measured tidal elevations at Bayou Rigaud collected by U.S. Coast Guard, Grand Isle. (Note different scales on ordinate axes.) Symbols along horizontal axis are as follows: ◐ = first lunar quarter; N = moon farthest north of equator; P = moon at perigee; ○ = full moon; E = moon on equator; ◑ = last lunar quarter; S = moon farthest south of equator; A = moon at apogee; ● = new moon. Dates are for January and February 1974.

The times of frontal passage were determined using National Weather Service weather maps; wind shifting at the Chevron rig, Boothville, and New Orleans; dry bulb and wet bulb temperatures at Boothville; atmospheric pressure at Boothville; and times of precipitation at Boothville and New Orleans.

Nearly every wind shift produces large hodographs, which diminish in size through a period of 1 to 4 days. A front on 3 February was followed by large hodographs on 4 through 6 February. A wind shift on 9 February was followed by several days of large shrinking hodographs during equatorial tides. On 18 February a front produced fairly well behaved rotary currents for a day. The wind shift of 20 February produced a nearly circular hodograph. The front on 21 February and wind shift on the 22nd produced a well-defined hodograph. Finally, a front on 24 February seems responsible for the strong rotary currents that follow on 25 and 26 February, a time of equatorial tides. Possibly the only exception to this pattern is the hodograph of 16 February, which follows the front of 15 February and shows rather poorly behaved clockwise rotary motion.

The evidence suggests that band-passed data contain rotary currents that are induced partially, if not in the most part, by wind. In the reminder of this paper an attempt will be made to demonstrate that these are indeed inertial oscillations of the surface layer.

C. Complex Demodulation of Observed Currents

A rotating current having both clockwise and counterclockwise components at many different frequencies may be expressed as

$$u(t) = \int_{-\infty}^{\infty} A(\omega) \exp(-i\omega t)\, d\omega \tag{17}$$

where $A(\omega)$ is the complex amplitude of the current at radian frequency ω and t is time. For the case of a current signal dominated by inertial oscillations, we assume that $A(\omega)$ is sharply peaked near $\omega = f$. Complex demodulation (Tukey, 1961; Perkins, 1970; Bloomfield, 1976) of this signal using f, the theoretical inertial frequency, as the demodulating frequency yields

$$\begin{aligned} U(t) &= u(t) \exp(\, ift) \\ &= \int_{-\infty}^{\infty} A(\omega) \exp(-i\omega t) \exp(\, ift)\, d_{\omega} \\ &= \int_{-\infty}^{\infty} A(\omega) \exp[\, i(f-\omega)t\,]\, d_{\omega} \quad . \end{aligned} \tag{18}$$

In trigonometric form, equation 18 is

$$U(t) = \int_{-\infty}^{\infty} A(\omega)\, [\cos(f-\omega)t + i \sin(f-\omega)t]\, d_{\omega} \quad . \tag{19}$$

Low-pass filtering of this signal will have one of two effects:

1. If ω is close to f, the amplitude of the signal, $A(\omega)$, will be relatively unchanged because the signal's frequency will be low.

2. If ω is not close to f, a high-frequency signal will result and it will therefore be eliminated.

The result of low-pass filtering yields the demodulated signal

$$U_D(t) = \int_{-\infty}^{\infty} A(\omega)\, G(\varepsilon)\, \exp(i\varepsilon t)\, d\omega \tag{20}$$

where $G(\varepsilon)$ is the transfer function of the low-pass filter and $\varepsilon = f - \omega$. It is desirable to use a filter that will not alter the phase of the output signal. A two-sided filter having symmetrical weights has such a property. One such filtering function is the equally weighted "running mean" or "moving average," whose transfer function (Holloway, 1958) is given by

$$G(\omega) = (\sin \omega T)/\omega T \tag{21}$$

where T is the half-width of the filter in the time domain. Thus, for $\omega \to f$, $\varepsilon \to 0$, $G(\varepsilon) \to 1$, $\exp(i\varepsilon t) \to 1$, and $U_D(t) \to A(f)$.

What the technique accomplishes, then, is to transform a signal at frequency ω, which may be concealed by large contributions at other frequencies, to a demodulated signal having a much reduced frequency of ε, which, when plotted, is more readily apparent to the eye. The demodulated current has a phase implicit in the complex amplitude $A(\omega)$ defined as $\phi = \tan^{-1}\{\mathrm{Im}[A(\omega)]/\mathrm{Re}[A(\omega)]\}$.

Complex demodulation may also be thought of as a local version of harmonic analysis in that it is a means to describe a signal at a given frequency in terms of its amplitude and phase. It is local in the sense that it describes these parameters in the neighborhood of a particular time, t, rather than for the entire record. In this study, a filtering interval of two inertial periods was chosen, i.e., T = 1 inertial period. Therefore, each $U_D(t)$ computed is a function only of those currents observed over the time period $t \pm 1$ inertial period and is independent of all other observed current velocities.

Demodulation of the February current record yields some interesting results (Fig. 7) when compared with the wind record. At first glance, there is an excellent correlation between rapid shifts in the wind direction (usually associated with fronts) and peaks in the amplitude of the demodulated current. Furthermore, these peaks are generally accompanied by a flattening of the plot of the phase of the demodulated current, indicating a signal of inertial or near-inertial frequency.

Because the inertial and diurnal tidal periods are so close, tidal currents will unfortunately also be preserved in the demodulated signal with little change in magnitude. However, because the peaks in current magnitude on Figure 7 all appear to be associated with specific wind events, it seems unlikely that tidal currents contribute substantially to the demodulated current. Furthermore, if the peaks in magnitude were tidal rather than inertial, then the associated phase would have a constant rate of change associated with each magnitude peak and presumably for the entire record. This is clearly not the case in Figure 7 or 8.

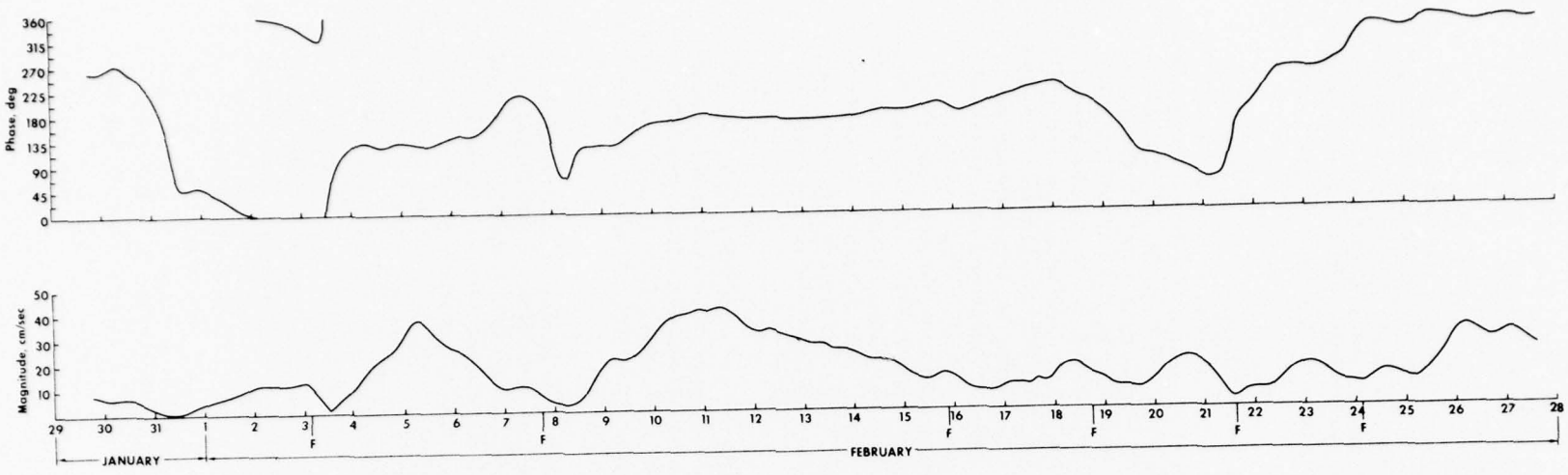

Figure 7. February demodulated current. The F indicates approximate times of frontal passage.

These points will be discussed further in connection with specific peaks in the current magnitude.

There are three prominent broad peaks in the amplitude, centered on 5, 11, and 26 February, that have remarkably constant phase. Some of the less prominent peaks have a phase that is slowly changing; a rotation of the current vector either faster or slower than inertial is suggested. An increasing phase, as defined here, indicates that the current vector's period of rotation is less than inertial, whereas a decreasing phase results from a vector's rotating with a period greater than inertial.

There are two possible features in a wind field that are very effective in generating or changing the amplitude of inertial oscillations: (1) a strong wind accompanied by a fairly sudden shift in direction or (2) a wind vector rotating clockwise for up to half an inertial period (Pollard and Millard, 1970; Pollard, 1970). As an example of case 1, consider a wind stress acting in one direction for an arbitrary period of time. Such a wind adds momentum to an inertial current during the first half of each inertial period and removes it during the second half. Therefore, a wind that suddenly changes direction or is removed at the end of 1/2, 3/2, 5/2, etc., inertial periods produces maximum inertial amplitudes. For case 2, if a wind vector rotates clockwise at inertial frequency, it continuously adds momentum to an inertial current, thereby continuously increasing its amplitude.

Both conditions are usually present in varying degrees when an atmospheric front approaches or passes a given site. Along the Louisiana coast, an approaching front is normally accompanied by a relatively slow clockwise rotation of the wind, which blows first from the east, then from the south, and, finally, as the front passes, suddenly shifts to the west or northwest. The passage of the front satisfies case 1, whereas wind conditions accompanying the approach of the front satisfy case 2.

Another example of case 2 can occur without the presence of a front as a result of the geometry of the isobars. For example, a high-pressure system whose center passes north of an oceanic site toward the east has clockwise rotating winds. Depending on the rate at which the system moves, the rotation rate of the accompanying winds may approach inertial frequency. However, a clear example of this situation is not present for the time period of this study.

Another factor that is crucial in determining the amplitude of the wind-induced oscillations near 30° latitude is the magnitude and direction of the diurnal tidal current. If, for example, the tidal current has a component opposite a wind vector component for any period of time, momentum will be removed from the current field. The result will be diminishing or destruction of rotary motion. If, on the other hand, the wind and tidal current vectors each have a component acting in the same direction, momentum will be added to the current and rotary motion will be enhanced. The same arguments hold for pre-existing inertial motion at the time of a wind event.

It is instructive to compare wind strength and duration with the amplitude of the current peaks. For example, the peaks of 11 and 18 February are associated with generating winds of approximately equal strength but different duration. The wind on 9 February peaks sharply and rotates at inertial frequency, and truly strong winds occur for about 12 hours. The wind of 18 February shifts rapidly but becomes unidirectional and still strong on 19 February, and the peak lasts about 24 hours. Results of the two events are quite different. The wind event of 9 February increases the already existing oscillations by about 20 cm/sec, whereas the peak

produced on 18 February is only 7 cm/sec above the background and is eliminated by the strong unidirectional wind of 19 February.

Winds following the front of 24 February produce some interesting amplification as well as destruction of inertial motion. Following the wind shift in the early morning of 24 February, inertial current amplitude built for half the inertial period and then diminished for the second half of the period. Very slow rotation of a strong wind vector following the wind shift seems to be responsible. Strong amplification of the inertial current during 25 February and early 26 February for somewhat less than an inertial period was caused by a moderate to strong wind vector that rotated slowly clockwise. Because February is a time of equatorial tides, lunar effects are minimal and therefore the motion must be considered inertial. There is some destruction and then amplification for about 1/2 inertial period following the maximum current of early 26 February. The phase of the demodulated current shows a nearly constant value from early 25 February to the end of the record; a frequency very close to inertial is indicated.

According to the meteorological data from the Weather Bureau station at Boothville, the front of 3 February is accompanied by a strong narrow peak in the wind speed and followed by several days of relative calm. (Unfortunately, the anemometer at the Chevron rig was not activated until 4 February). There is an associated strong uniform increase in the demodulated current with a constant phase. Tidal effects might seem significant because of closeness to the time of tropic tides. However, the moon is at its maximum declination on 2 February and the demodulated current for that day is only 10 cm/sec as compared with the peak of 40 cm/sec on 5 February, following the front of 3 February. The time lag between maximum lunar declination and resulting tropic tide, the so-called "age" of the tropic tide, along the Louisiana coast is about 6 hours (Marmer, 1954). As a result, the peak of 5 February occurs much too late to be the result of the lunar effects of 2 February.

Peaks in the demodulated current for the period 15 to 24 February are relatively small and of short duration. From the nature of the wind during this time interval, it appears that wind stress is as important a factor in the decay of the currents as it is in their generation. Each peak has a decay time of 12 to 24 hours which in each case corresponds to a period of fairly unidirectional wind lasting 12 to 24 hours. Consider, for example, the peak centered on 23 February. The wind shift that begins on 22 February is followed on 23 February by light winds toward the west. The inertial current on 23 February shows a uniform decrease in amplitude. This decrease suggests that wind stress is tending to remove momentum from the current system.

Furthermore, the close spacing of strong wind episodes during this period seems to preclude the observation of long-duration, strong inertial amplitudes in the current. Spacing of wind shifts and fronts, with the exception of the one on 15 February, is about one to two inertial periods, a time interval that is rather short when one wishes to resolve well this type of rotary motion.

In order to further substantiate the conclusions drawn from the demodulation of the February current record, a current time series extending from 25 April through 2 June was also subjected to complex demodulation. Figure 8 shows only one major peak in the demodulated current centered on 12 May and associated with a frontal passage early on 11 May that exhibited gusts of up to 21 m/sec. Although weather maps for this time period indicate the passing of four fronts, weather data from Boothville indicate that the front of 11 May was by far the strongest, the others being fairly diffuse and generally barely perceptible in the study region. There is some correspondence between the shifting of the wind at Boothville and

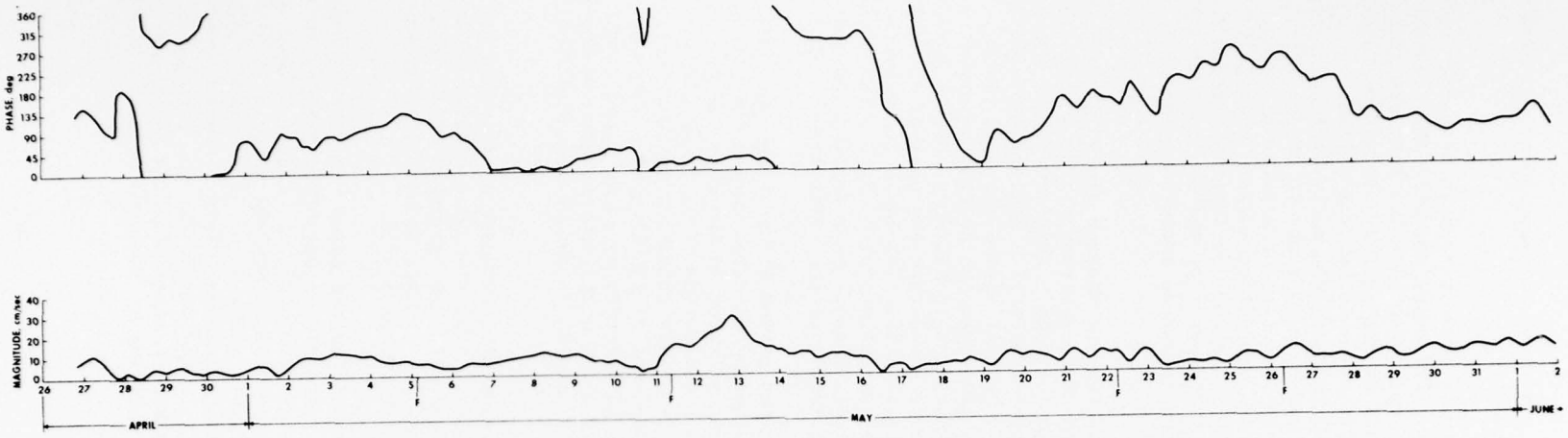

Figure 8. May demodulated current. F indicates approximate time of frontal passage. Weather data indicate that only the front of 11 May was significant.

the small current peaks, but it is difficult to characterize these as inertial owing to their relative weakness. In fact, this record seems to be indicative of background tidal noise for this region. On the basis of this record, a fairly representative value for maximum tidal current magnitude is on the order of 10 cm/sec.

D. Spectral Analysis

The Fourier transform (Blackman and Tukey, 1959) of a finite-duration time series x(t) is given by

$$X(\omega) = \frac{1}{T} \int_{-T/2}^{T/2} x(t)\, e^{-i\omega t}\, dt, \qquad -T/2 \leq t \leq T/2 \tag{22}$$

where T is the duration of the series, ω is radian frequency, and t is time.

The correlation function for components u and v of a finite-duration vector time series is given by

$$R_{uv}(\tau) = \frac{1}{T} \int_{-T/2}^{T/2} u(t)v(t + \tau)\, dt \tag{23}$$

where τ denotes a time lag. The symbol R_{uv} represents the cross correlation. Similarly, R_{uu} and R_{vv} may be used to express autocorrelations of u and v, respectively.

The two-sided spectrum is defined by the Fourier transform of the correlation function

$$S_{uv}(\omega) = \int_{-\infty}^{\infty} R_{uv}(\tau)\, e^{-i\omega\tau}\, d\tau \tag{24}$$

for $-\infty < \omega < \infty$. This quantity is referred to as the cross-spectrum of series u and v. We may similarly compute S_{uu}, the autospectrum of u, from R_{uu}, and S_{vv}, the autospectrum of v, from R_{vv}. These are commonly termed the power spectra of u and v, respectively.

Conventional analysis of time series usually deals with the so-called "physically realizable one-sided spectra," which, as defined by Bendat and Piersol (1966), are

$$\begin{aligned} P_{uu}(\omega) &= 2S_{uu}(\omega) \\ P_{vv}(\omega) &= 2S_{vv}(\omega) \\ P_{uv}(\omega) &= 2S_{uv}(\omega) \end{aligned} \tag{25}$$

where the spectra are now defined for $0 < \omega < \infty$. The cross spectrum can further be divided into a real part, C_{uv}, called the cospectrum, and an imaginary part, Q_{uv}, called the quadrature spectrum, expressed as

$$P_{uv}(\omega) = C_{uv}(\omega) - iQ_{uv}(\omega) \tag{26}$$

for $0 < \omega < \infty$.

According to Bendat and Piersol (1966), Q_{uv} is an odd function of ω, i.e., $Q_{uv}(\omega) = -Q_{uv}(\omega)$, and $P_{uu}(\omega)$ and $P_{vv}(\omega)$ are even functions, i.e., $P_{uu}(-\omega) = P_{uu}(\omega)$ and $P_{vv}(-\omega) = P_{vv}(\omega)$. Using the quantities in equations 25 and 26, Gonella (1972) writes for the one-sided counterclockwise spectrum

$$S_+ = \frac{1}{4} [P_{uu}(\omega) + P_{vv}(\omega) + 2Q_{uv}(\omega)] \tag{27}$$

For the one-sided clockwise spectrum,

$$S_- = \frac{1}{4} [P_{uu}(\omega) + P_{vv}(\omega) - 2Q_{uv}(\omega)] \ . \tag{28}$$

The total spectrum is

$$\begin{aligned} S_t(\omega) &= S_- + S_+ \\ &= \frac{1}{2} [P_{uu}(\omega) + P_{vv}(\omega)] \ . \end{aligned} \tag{29}$$

We may now write the difference between the two spectra:

$$S_- - S_+ = -Q_{uv}(\omega) \tag{30}$$

The sign of this quantity represents the polarization of energy in the clockwise sense for positive sign and counterclockwise for negative (Gonella, 1972).

The ratio

$$C_R = (S_- - S_+)/S_t(\omega) = -2Q_{uv}(\omega)/[P_{uu}(\omega) + P_{vv}(\omega)] \ , \tag{31}$$

called the rotary coefficient (Mooers, 1973; Gonella, 1972; Fofonoff, 1969), gives a measure of the partition of total spectral energy $S_t(\omega)$ between clockwise and counterclockwise rotating components. Its value is zero for unidirectional motion, -1 for pure counterclockwise rotary motion, and +1 for pure clockwise motion.

Spectra for the data set were computed with the Cooley-Tukey Fast Fourier Transform (FFT). A potentially troublesome aspect encountered when using the FFT stems from the fact that the time series being analyzed is finite. The FFT "assumes" that a given signal repeats itself infinitely in time (W. Wiseman, 1976, personal communication). Therefore, if a given time series contains sinusoidal components

and the record to be analyzed is such that the beginning and the end of the record do not correspond to the same point on the sine curve, the ends of the record will be interpreted as discontinuities. A strong high frequency flattening in the spectrum may be produced. However, the problem can be circumvented by tapering the ends of the time series. The February current record was linearly detrended and tapered over 10 percent of the record at the beginning and the end of the time series using a cosine bell, as suggested by Brigham (1974).

The FFT algorithm has certain advantages over the computing of spectral estimates with the time-lagging method. For example, the number of spectral estimates that it can compute is equal to half the number of data points, whereas one is restricted in the lagging technique to about 10 percent of the number of data points. The FFT, therefore, achieves considerably better frequency resolution. Its limiting frequency, the Nyquist frequency, $f_N = 1/2\Delta t$, where Δt is the data interval, represents the highest frequency for which spectral information may be obtained. An important advantage in statistical analysis is the fact that the estimates computed by the FFT are nearly statistically independent. Finally, it is highly efficient in terms of computer time when compared with other techniques for obtaining the same amounts of information.

In using the FFT, we write equation 24 in its alternate form (Lathi, 1968)

$$S_{uv}(\omega) = \left[\frac{1}{T}\int_{-T/2}^{T/2} u(t)\, e^{-i\omega t}\, dt\right]^* \cdot \frac{1}{T}\int_{-T/2}^{T/2} v(t)\, e^{-i\omega t}\, dt \qquad (32)$$

where the asterisk denotes the complex conjugate of the Fourier transform. We next define real and imaginary Fourier coefficients $a(\omega)$ and $b(\omega)$ for $u(t)$ and $c(\omega)$ and $d(\omega)$ for $v(t)$, which may be used to express the cross spectrum in terms of trigonometric functions (Lathi, 1968). Therefore, dropping the functional notation (ω) from $a(\omega)$, $b(\omega)$, $c(\omega)$, and $d(\omega)$,

$$\left[\frac{1}{T}\int_{-T/2}^{T/2} u(t)\, e^{-i\omega t}\, dt\right]^* = (a + ib)/2$$

$$\frac{1}{T}\int_{-T/2}^{T/2} v(t)\, e^{-i\omega t}\, dt = (c - id)/2 \quad . \qquad (33)$$

The two-sided cross spectrum is then

$$S_{uv}(\omega) = [ac + bd + i(bc - ad)]/4 \quad . \qquad (34)$$

Finally, the one-sided autospectra are

$$P_{uu}(\omega) = 2S_{uu}(\omega) = (a^2 + b^2)/2$$

$$P_{vv}(\omega) = 2S_{vv}(\omega) = (c^2 + b^2)/2 \qquad (35)$$

and one-sided cospectrum and quadrature spectrum are, respectively, the real and imaginary parts of S_{uv}.

$$C_{uv}(\omega) = 2\mathrm{Re}\ [S_{uv}(\omega)] = (ac + bd)/2$$

$$Q_{uv}(\omega) = 2\mathrm{Im}\ [S_{uv}(\omega)] = (bc - ad)/2 \tag{36}$$

where $0 < \omega < \infty$.

The various spectral quantities were computed using the FFT, and, from these, values of C_R were calculated at all frequencies. Table 3 lists some values of the rotary coefficient, as well as the clockwise and counterclockwise spectral energy for frequencies near the inertial-diurnal and semidiurnal frequencies. As expected, the major clockwise spectral peaks occur in the inertial-diurnal region. These particular frequencies also generally have a $C_R > 0.9$ and $C_R > 0.99$ immediately above the inertial and diurnal frequencies. The lack of a stronger spectral peak in the semidiurnal tidal frequency is rather surprising in view of the fact that the tide for the Louisiana coast is semidiurnal for part of the month. Also surprising are the values of C_R in the vicinity of the semidiurnal frequency. The values indicate nearly unidirectional motion instead of the expected clockwise polarization. At least for this record, it must be concluded that the semidiurnal tidal component makes no significant contribution to rotary motion for the region being studied.

Figure 9 shows the counterclockwise, clockwise, and total spectra. Except for rather minor spikes, there is no significant energy in any of the spectra in the vicinity of the semidiurnal tidal frequency. The counterclockwise spectrum contains significant energy only at the lowest frequencies; spectral energy drops off fairly uniformly for the higher frequencies. As expected, energy in the clockwise and total spectra is concentrated in a major peak near the inertial-diurnal frequencies. By far the strongest peak in S_- and S_t occurs at a frequency of 0.043 CPH, corresponding to a period of 23.26 hours. There are four less energetic peaks in the vicinity associated with frequencies of 0.031, 0.035, 0.049, and 0.053 CPH (periods of 32.26, 28.57, 20.41, and 18.87 hours, respectively).

Substantial energy is present in all three spectra for very low frequencies. This energy is apparently associated with a mean flow in the region.

The strongest peak, representing inertial-tidal frequencies, occurs at a somewhat higher frequency than theory indicates for inertial currents and is spread over a band of frequencies. Gonella (1971) similarly observed a shorter period of inertial rotation over a band of frequencies at the Bouée Laboratoire in the Mediterranean. The phenomenon results from the rotary motion at various depths in the water layer tending toward the inertial frequency.

Let us assume that at some arbitrary time, $t_o = 0$, a wind stress acting at the surface is suddenly removed and the resulting vertical current distribution is given by $u_o(z)$. The vertically integrated velocity distribution, R_o, at time t_o is then

$$R_o = \int_{-\infty}^{o} u_o(z)\, dz \tag{37}$$

Table 3

Spectral Estimates and Rotary Coefficient near the Inertial-Diurnal and Semidiurnal Frequencies for the February 1974 Current Record

Frequency (CPH)	S_- $((cm/sec)^2/CPH)$	S_+ $((cm/sec)^2/CPH)$	C_R
0.027	2.173	0.449	0.658
0.028	1.110	0.376	0.494
0.030	2.692	0.588	0.642
0.031	10.635	0.383	0.930
0.032	6.041	0.305	0.904
0.034	2.515	0.428	0.709
0.035	10.908	0.071	0.987
0.036	5.461	0.450	0.848
0.038	0.437	0.718	-0.243
0.039	2.986	0.777	0.587
0.041	22.092	0.423	0.962
0.042	27.264	0.045	0.997
0.043	53.460	0.207	0.992
0.045	4.921	0.013	0.994
0.046	3.427	0.465	0.761
0.047	6.956	0.274	0.924
0.049	15.422	0.473	0.940
0.050	7.561	0.383	0.904
0.051	6.517	0.043	0.987
0.053	10.965	0.139	0.975
0.054	0.064	0.076	-0.087
0.055	2.298	0.206	0.836
--	--	--	--
--	--	--	--
--	--	--	--
0.076	0.061	0.228	-0.578
0.077	0.431	0.193	0.382
0.078	0.254	0.150	0.258
0.080	0.172	0.205	-0.087
0.081	0.044	0.044	-0.005
0.082	0.432	0.414	0.021
0.084	0.126	0.135	-0.032
0.085	0.412	0.183	0.385
0.086	0.006	0.004	0.213
0.088	0.129	0.058	0.380
0.089	0.078	0.185	-0.407
0.091	0.099	0.031	0.526

Next, define a current velocity $u(z,t)$ for $t > 0$ and $R(t)$, the integrated velocity vector, such that

$$R(t) = \int_{-\infty}^{0} u(z,t)\, dz \tag{38}$$

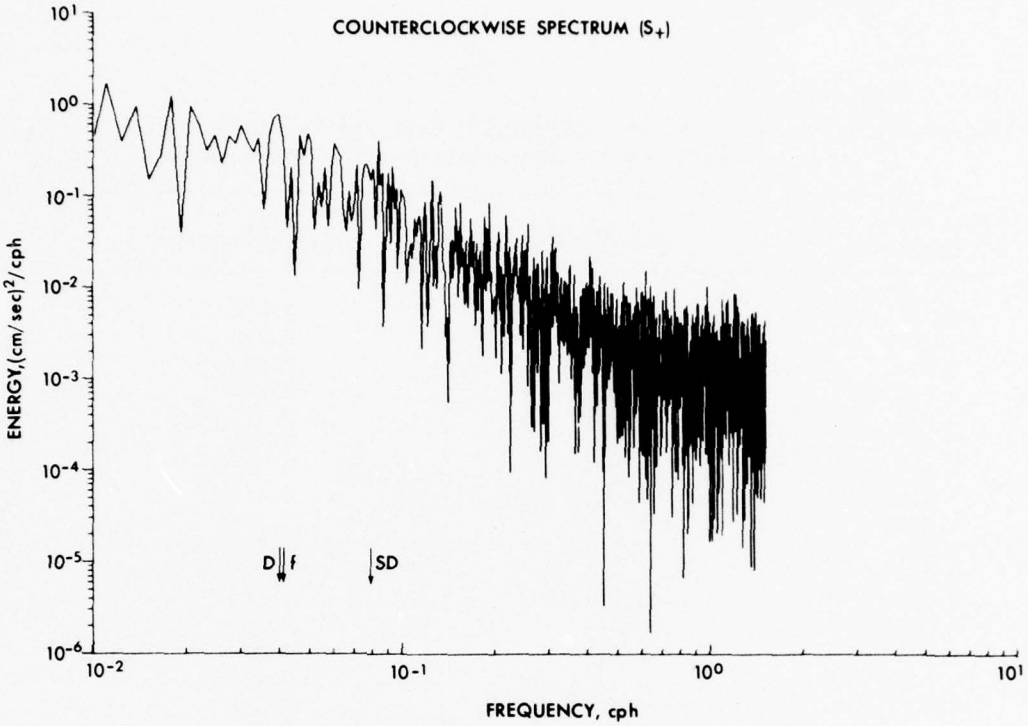

Figure 9A. Counterclockwise spectrum of the February 1974 current record. D, f, and SD represent *diurnal tidal frequency*, *inertial frequency*, and semidiurnal tidal frequency, respectively.

The vector R(t) tends to decay in amplitude under the influence of viscosity and to rotate at the natural frequency of the system, i.e., the inertial frequency. If at a given depth, z, $u_o(z)$ leads R_o, then for $t > 0$ the period of rotation of u(z,t) is less than the inertial period as u(z,t) tends to R(t); if $u_o(z)$ lags behind R_o, the period of rotation of u(z,t) is greater than the inertial period (Gonella, 1971). In either case, the inertial period is approached in the limit at each depth. Gonella's solution (Gonella, 1971) for a wind stress imposed at $t_o = 0$, as well as for a duration-limited wind stress, predicts the same approach of the rotation period to the inertial period. Figure 10, adapted from Gonella (1971), illustrates this point. Gonella (1971) noted that the action of viscosity explains in part peaks in his spectrum for $f' - f \pm 2$ to 4%, where f' is observed frequency. The same mechanism seems to be responsible for the spectral peak spanning the frequencies 0.041 to 0.043 CPH, which are within $f' = f + 6\%$.

Modification of the period of inertial rotation may result from a number of conditions, among which are mass stratification or the presence of horizontal mean flow (Gonella, 1971; Perkins, 1972). The latter may create a Doppler shift in the observed frequencies. Perkins (1972) noted a frequency of rotation 3 percent above the theoretical f because of the presence of a mean current. Gonella (1971) observed similar frequency shifting in three examples of inertial motion. Pollard's (1970) wind-driven model for a two-layered ocean predicts frequencies in the inertial current in the range $f < f' < 1.07\ f$. The fact that in this particular study

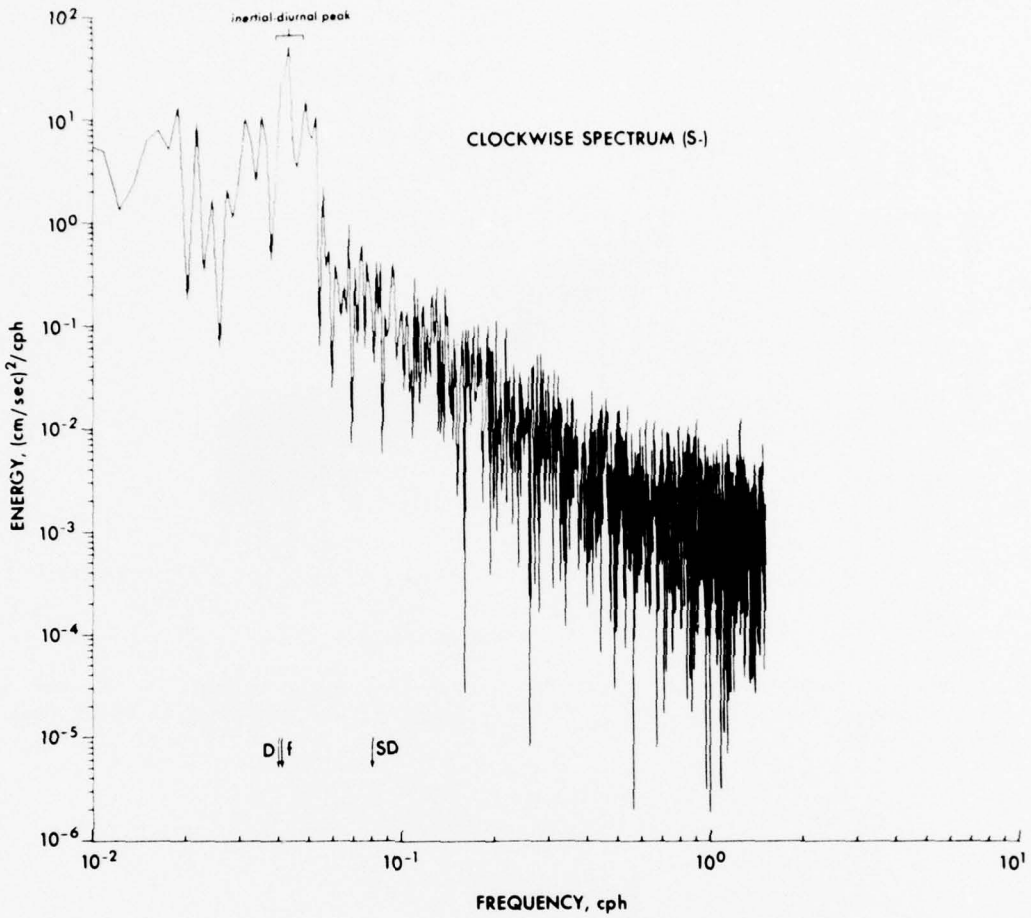

Figure 9B. Clockwise spectrum of the February 1974 current record. Inertial-diurnal peak is indicated at top. D, f, and SD represent diurnal tidal frequency, inertial frequency, and semidiurnal tidal frequency, respectively.

the major spectral peak occurs at a frequency 6 percent above inertial is not surprising.

Stratification probably contributes to some extent to the frequency shifting. Stratification of waters in the study site is not uncommon because of land runoff and Mississippi River discharge. This stratification, as well as the presence of mean flow, operates in a rather complex fashion that is difficult to define quantitatively. For this reason, shifting of the inertial frequency is usually treated in the literature only in a very general and qualitative manner (see, for example, Perkins, 1972; Gonella, 1971).

Although the major peak at 0.043 CPH may be explained by the effects of mass stratification and Doppler shifting of the inertial frequency, the reason for the four minor peaks at 0.031, 0.035, 0.049, and 0.053 CPH is not as clear. On the basis of available data, it is difficult to make definitive conclusions as to their cause. However, it does seem likely that they may be a result of some property of

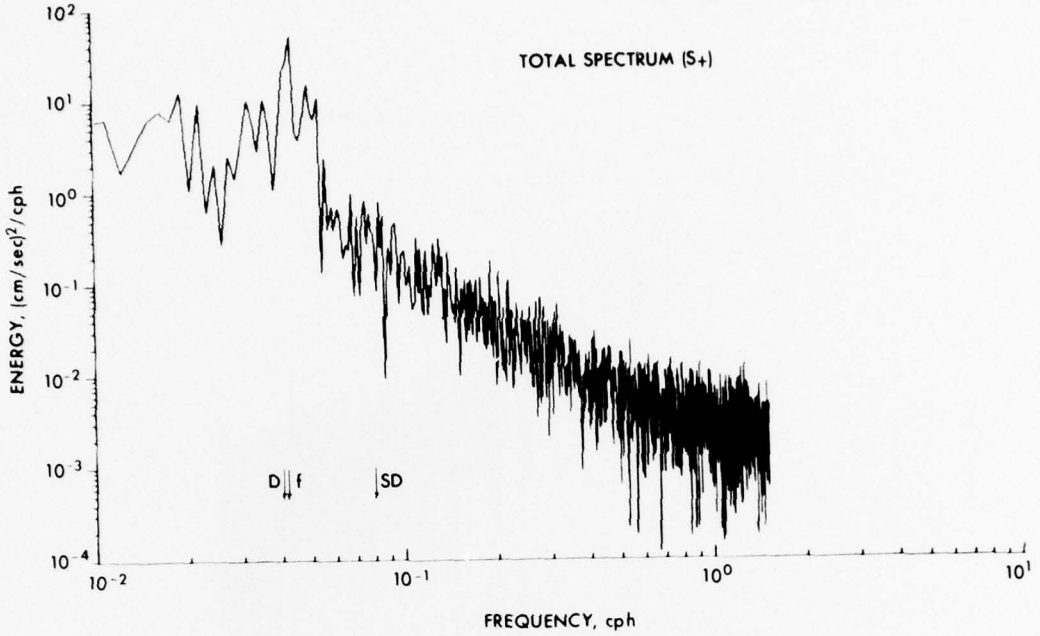

Figure 9C. Total spectrum of the February 1974 current record. D, f, and SD represent diurnal tidal frequency, inertial frequency, and semidiurnal tidal frequency, respectively.

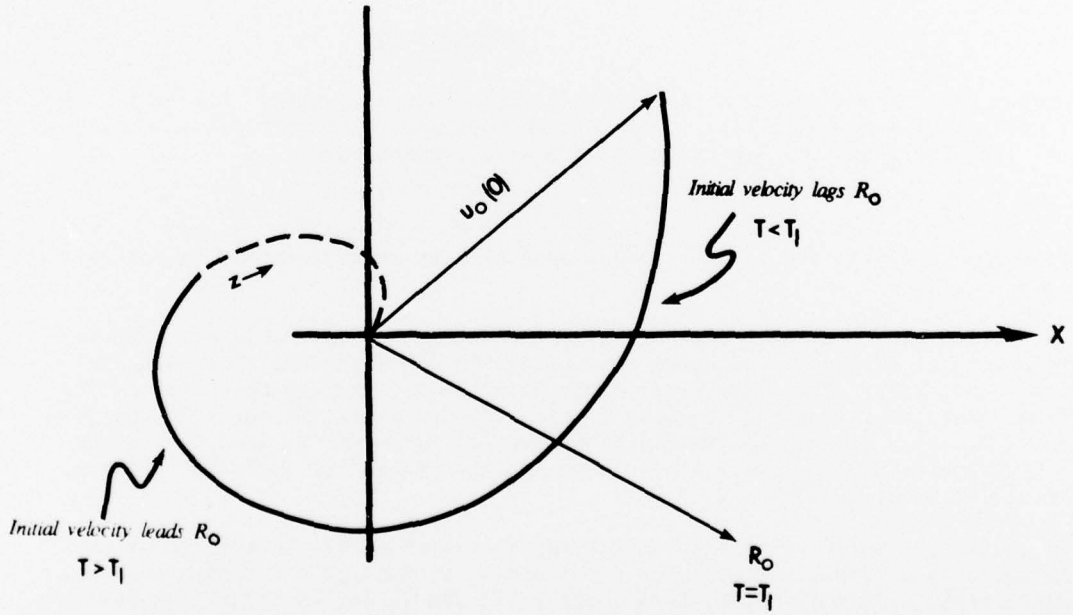

Figure 10. Projection of Ekman spiral on a horizontal plane. Rotation period for $u(z,t)$ above R_0 is less than inertial, and below R_0 it is greater than inertial. (Adapted from Gonella, 1971.)

the wind field. Each of the four frequencies has an associated $C_R > 0.93$, suggesting strongly polarized clockwise motion. The four peaks may, therefore, represent driving by a clockwise rotation of a strong wind. Each of the four frequencies suggests a separate wind event and strong energy at a particular frequency.

E. Simulation of Wind-Induced Currents with the Pollard-Millard Model

Pollard and Millard (1970) were able to account for wind-stress-induced inertial currents in the surface layers of the open ocean with a mathematically simple model. They assumed a homogeneous surface layer of uniform depth on an f-plane. Rather than treating the wind stress as a surface boundary condition, they assumed it to be instantaneously and uniformly distributed through the mixed layer of depth Z, i.e., as a body force. This particular modeling of the wind stress is justified for two reasons (Pollard, 1970):

1. The depth of the well-mixed surface layer created by applying a surface stress increases as $t^{1/3}$ (Kato and Phillips, 1969), where t is time. On the other hand, the time scale for transmitting momentum through the well-mixed layer several tens of meters deep is on the order of several hours. Therefore, the time scale for spreading the momentum through the mixed layer is short compared with the inertial period, but the time scale of the deepening of the layer is considerably longer than the inertial period. Consider, for example, a constant wind stress of $\tau = 4$ dynes/cm^2 applied at the surface of a strongly stratified layer of Brunt-Väisälä frequency $N = 10^{-2}$ sec^{-1}. Kato and Phillips' formula states that the mixed depth Z(t) is given by $Z(t) = u_* (15t/n^2)^{1/3}$, where $u_* = (\tau/\rho_w)^{1/2}$ is the friction velocity, t is time, and ρ_w is water density. A wind stress of 4 dynes/cm^2 would erode such a stratified fluid down to 20 m in less than 2 hours. On the other hand, the rate at which Z(t) increases is given by the derivative of the above equation, $dZ(t)/dt = 0.82\ u_*/(tN)^{2/3}$. After 6 hours, the constant wind stress deepens the layer at a rate of 1.6 m/hr; after 12 hours, that rate decreases to 1 m/hr. In other words, the time required for the bottom of the surface layer to "feel" momentum applied at the surface is at least an order of magnitude shorter than the time for the depth of the layer bottom to increase substantially. Instantaneous transmission of surface stress through the surface layer is therefore a valid assumption.

2. A weakly stratified layer cannot sustain a strong vertical velocity shear and therefore will have a tendency to have momentum uniformly distributed through it. Homogeneous distribution of momentum from the surface, where stress is applied, to a depth Z is thus a valid assumption.

The vertically averaged, linearized equations of motion in the mixed layer are:

$$\frac{\partial u}{\partial t} - fv = F - ku$$

$$u,\ v \equiv \frac{1}{Z}\int_{-Z}^{0} (u', v')\, dz \qquad (39)$$

$$\frac{\partial v}{\partial t} + fu = G - kv$$

where u' and v' are point measurements of the current and u and v represent their vertical averages and F and G are the forcing functions (in this case, wind stress) in the x and y directions, respectively. The F and G time series are here defined

as

$$(F_i, G_i) = \frac{\rho_a C_D U_i^2}{\rho_w Z} (\sin \theta_i, \cos \theta_i) \qquad (40)$$

where $U_i \sin \theta_i$ and $U_i \cos \theta_i$ are the 1-hour vector averages of wind velocity components for hours i = 1, 2, 3,...n, ρ_a and ρ_w are the density of air and water, respectively, Z is the depth of the mixed water layer, and C_D is the drag coefficient (= 1.2×10^{-3} (Hsu, 1974)). The linear damping terms -ku and -kv introduce an exponential decay factor into the solution of equations 39 (see "Introduction"). The constant k^{-1}, referred to as the e-folding time, describes the time required for the rotary current to be dissipated by viscosity to e^{-1} of its original value. If $k^{-1} = T$, where T is an arbitrary period of time, then after a time t = T we have the current speed V(t) related to the initial speed by $V(t) = V_o e^{-(1/T)T} = V_o e^{-1}$. Equations 39 were solved iteratively by Pollard and Millard using a time step of 1 hour. Considering the simplicity of the model, the predicted currents they obtained show striking similarity to those observed.

The Pollard-Millard model was used to generate currents from Weather Bureau wind data at Boothville for 28 January to 4 February and winds from the Chevron rig for 4 through 28 February. Profiles of temperature and salinity near the moored meter at the beginning and the end of this period indicate a fairly well mixed surface layer down to about 10 meters for the current record. Several values of the e-folding time were tried in order to obtain the best possible correspondence between observed and modeled current amplitudes.

Keeping in mind the points made in Section II-C about properties of the wind field that initiate or destroy inertial motions, a comparison of wind (Fig. 11A) with the observed and modeled current (Fig. 11B) reveals several examples of wind-generated oscillations. The best example of this phenomenon is the very regular sinusoidal oscillation of the u and v components of the observed current beginning on 9 February and continuing for nearly a week. The model is highly successful in reproducing these observed oscillations. A significant feature of the modeled current is the fact that it is in phase with the measured current immediately following a wind event but gradually drifts out of phase. Pollard and Millard (1970) noted that the dominant frequencies of the model and the ocean are slightly different, and therefore the two will drift out of phase when there is little forcing. Furthermore, the damping factor, k, may change significantly with time, thereby altering the character of the observed oscillations. As a result, the model can be expected to give the best correlation with the observed current within a few days of a given wind event.

Figure 11B shows the comparison between the simulated current with 2-day damping ($k = 5.8 \times 10^{-6}$ sec^{-1}) and the observed current. The model reproduces with considerable accuracy nearly all the major features of the measured current for the period 4 through 28 February. It is not as successful over the period 28 January to 4 February for reasons to be discussed later.

On 9 February a moderately strong wind rotating nearly inertially in phase with the current continuously added momentum to the current for a 24-hour period. The result was the set of large-amplitude oscillations that gradually diminished in strength with time. Wind conditions following the wind shift on the 9th and continuing through the 15th were very conducive to maintaining the oscillatory motion; that is, after the 9th and up to the 15th the wind was weak and therefore there was little additional forcing to either enhance or destroy the current motion.

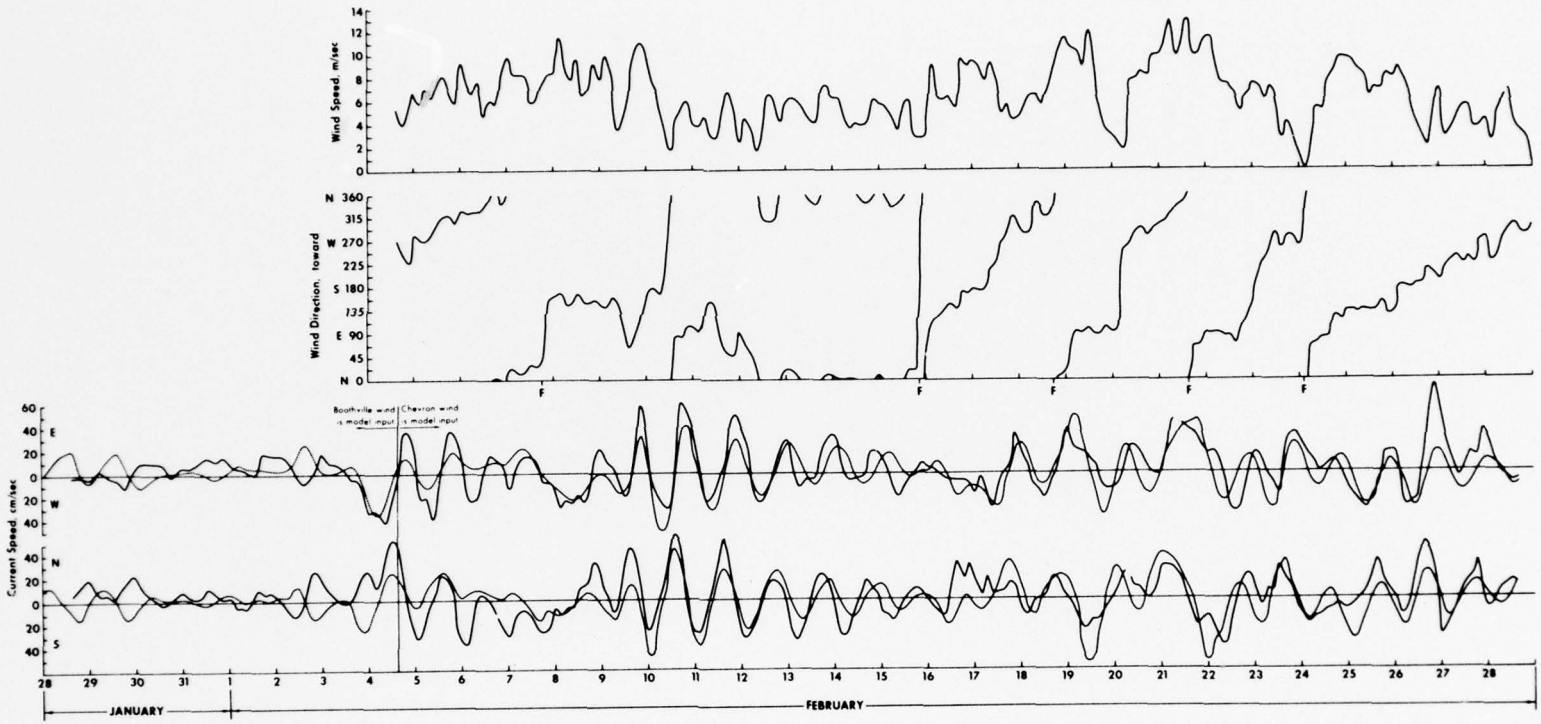

Figure 11. A. Wind record at Chevron platform. B. E-W and N-S components of observed (solid line) and simulated (dotted line) currents. F in A indicates approximate time of frontal passage. Simulated current from 28 January to the afternoon of 4 February was generated using Weather Bureau wind record at Boothville. From 4 to 28 February wind at the Chevron platform was used. Dates are for January and February 1974.

Without knowledge of the wind characteristics during this period, the observed oscillations might be assumed to be diurnal tidal motion. In fact, filtering with the Doodson-Warburg and binomial filters seems to indicate that this is indeed the case (see Fig. 5). However, the possibility that these are purely tidally driven motions must be ruled out because the tidal record at Bayou Rigaud (Fig. 6B), as well as the NOS-predicted tide for Caminada Pass (National Ocean Survey, 1974) (Fig. 6A), indicates relatively small and partially semidiurnal tidal amplitude for this period. The period corresponds to the time of equatorial tides, when tidal amplitude was at a minimum. It must be remembered that the Pollard-Millard model is a purely wind-driven model and therefore it cannot produce rotary tidal motion. The degree to which it accurately reproduces the observed oscillations of 9 through 15 February is strong evidence that the observed rotary motion was wind induced.

On 15 February a frontal passage late in the day was accompanied by a 360° turn in the wind vector over approximately a 6-hour period. Its effect was the destruction of whatever remained of the rotary motion induced by the 9 February wind event. The observed current on the 16th and 17th showed some semidiurnal variation that was not apparent in the simulated current. These may represent an effect of either the semidiurnal tide or turbulence.

Anticyclonic motion was created by a wind shift on 17 February and was somewhat enhanced by the front late on the 18th. Although this front initially produced moderate to strong currents, the oscillatory amplitude was diminished from noon on the 19th through midnight on the 20th. The reason is that the wind was very strong and nearly unidirectional for about one inertial period on the 19th. Wind during this period seems to have removed momentum from the current system.

On the afternoon of 21 February a front initially produced strong amplitudes in the current components that were followed by undulations of near-inertial period that lasted for about two and a half inertial periods. These undulations, however, were not as strong in amplitude as might have been expected if we examine the strength of the wind stress. As before, the reason appears to be the direction of the wind on the 21st and 22nd. The wind was unidirectional for nearly one inertial period beginning on the 21st and ending on the 22nd. It was therefore instrumental in diminishing the oscillatory amplitude.

A word of caution should be made at this point regarding the spacing of wind events and the oscillations they produce in the current components. As one approaches lower latitudes, the inertial period becomes increasingly long. At the latitude of the study site, this period is slightly longer than a day. If wind events occur one or two inertial periods apart, as is the case in the instance just mentioned, it becomes increasingly difficult to observe inertial motions. In the strict sense, inertial currents, once induced, are acted upon only by the deflecting force, Coriolis force. In real-world situations, inertial rotary currents, once induced, are acted upon by both internal and external forces, which may make their observation difficult. For example, if a front creates what appears to be inertial rotary motion and is followed within one or two inertial periods by another front and accompanying clockwise wind rotation, the current motion observed between frontal passages may not be inertial rotation but rather currents that are driven by the anticyclonically rotating wind vector associated with the second approaching front. As a result, characterization of the oscillations between times of the fronts of 21 and 24 February, for example, may be somewhat problematical because of the clockwise rotation of the wind on the 21st, which was followed by another rotation on the 22nd and a third on the 24th.

Strong-amplitude oscillations appearing in the observed current toward the end

of the record were induced by the front of 24 February. Winds during this period were generally weak to moderate and shifted very slowly clockwise. The degree to which the model is able to simulate the observations is only fair. Especially surprising is the magnitude of the observed current on 26 February, the strongest current of the entire study period. Although the model does produce significant undulations, it falls far short of creating the peak of 26 February. As was the case earlier in the record, tidally driven currents must be ruled out as a primary mechanism in producing the peak. The tide record at Bayou Rigaud shows relatively small tidal range for 25 to 27 February, as is the case with the NOS-predicted tide levels. This particular period was the time of equatorial tides and therefore tidal effects were minimal. The failure of the model to reproduce the strong magnitude of the rotary current of the 26th may possibly be explained by a significantly reduced friction coefficient, k, for about a day, but there are no data available to support this conjecture.

One final event worth mentioning is the front of 3 February. Unfortunately, recording of wind data at the Chevron rig was not begun until the afternoon of the 4th. The observed current components following the front show fairly well behaved strong oscillations, and it was therefore desirable to model them. Using 1-hour values of wind velocity collected by the Weather Bureau at Boothville, simulated currents were generated for the period before 4 February not covered by the Chevron wind data. A linear regression of the available Chevron wind data was performed on the Boothville wind data to compensate for differences in wind magnitude over land and over water. The results at 1500 hours on 4 February of modeling with the regressed wind data were used as initial current amplitudes for the model using the Chevron wind record. This procedure produced only marginally accurate results. Although undulations do occur in the simulated components beginning on 3 February, they do not adequately describe the well-defined oscillations of the observed components. In addition, currents before 4 February which are generated with the Boothville wind as input are a rather poor simulation. The problem stems from a number of causes, among which are (1) winds over land are deflected more from their geostrophic values than those over water and therefore wind direction at Boothville is probably not a good representation of direction over the current meter; (2) distance between Boothville and the moored current meter is too great to allow an adequate representation of wind conditions at the study site. Despite these difficulties the model indicates that the undulations in the current components observed for 4 or 5 days after the front of 3 February were wind-induced inertial oscillations.

III. SUMMARY AND CONCLUSIONS

Results of the various analyses performed on the current velocity time series suggest strongly that the rotary motion observed is locally wind-induced inertial oscillation and is not the result of astronomical tides. Evidence to support this conclusions is as follows:

1. The observed currents, plotted as a progressive vector diagram, clearly show clockwise rotation following significant wind shifts.

2. Conventional analysis using filters to extract tidal currents from the observed time series produces current hodographs that are totally unrelated to the predicted tide or to the measured tidal elevations. The size of the hodographs is, however, closely related to wind shifting usually associated with frontal passage.

3. Complex demodulation of the current time series indicates a large-magnitude signal near the inertial frequency that is closely associated with passing

fronts. The major peaks have a magnitude of 30-40 cm/sec, whereas the background magnitude is 0-10 cm/sec (see Fig. 7). For this particular study period, the latter is probably a good measure of the magnitude of rotary currents not induced by wind, that is, tidal currents. Furthermore, the phase of the demodulated current does not show a slow uniform decrease, as would be expected for tidal currents. Instead, it demonstrates the transient nature of locally wind-induced inertial oscillations. The phase achieves a constant value with each magnitude peak and is different for each of those peaks.

4. Spectral analysis indicates a strong peak in the inertial-diurnal frequency band. The record is not long enough to resolve the inertial and diurnal frequencies, but the peak appears to be too strong to be generated by tides alone.

5. The Pollard-Millard model, which uses wind stress as the sole input, gives an excellent reproduction of the observed current components. Oscillations are produced in the modeled current by shifting winds. Particularly significant is the agreement between modeled and observed current components following the wind shift of 9 February. The generally good agreement in magnitude of the modeled and observed currents indicates that wind forcing is considerably more important than tidal forcing in producing the observed rotary motion.

The generation of inertial oscillations by wind is dependent on two properties of the wind field: its duration and its rotation rate. A unidirectional wind generates inertial rotary motion during the first half of an inertial period and diminishes it during the second half. A wind vector rotating at the inertial frequency generates an inertial current and continuously increases its magnitude. The magnitude of inertial oscillations observed following a particular wind event is also dependent on clockwise rotary motion near the inertial frequency existing prior to the wind event. A particular observation of "inertial" motion may therefore represent an enhancement of inertial oscillations or diurnal tidal currents existing prior to a given wind event. Not only is the wind instrumental in generating inertial oscillations, it can also diminish or destroy them. If the wind vector has a component opposite the current vector, it will remove momentum from the current field. If the situation persists, clockwise rotary motion of the current is totally eliminated.

Inertial motion as depicted by the demodulated current (Figs. 7 and 8) is contaminated by diurnal tidal motion. Inasmuch as the inertial and diurnal tidal frequencies for the Louisiana coast are so close, complex demodulation is unsuccessful in separating the two. However, demodulation clearly shows that wind has a dominant effect in generating rotary currents in the inertial-diurnal frequency band. This effect is apparent when we examine the magnitude and phase of the demodulated current in the presence and absence of wind events. The conclusion may be further substantiated by examining the tide record for the region during the study period.

The closeness of the inertial and diurnal tidal frequencies also presents problems in the spectral analysis. The 32-day record examined here is not long enough to resolve the two frequencies as distinct spectrum lines. However, even with considerably better resolution, formidable problems would be encountered. As pointed out in Section II-D, inertial motion is observed not at a single frequency but over a band of frequencies near the theoretical inertial frequency. This "smearing" of current energy over a frequency band, as pointed out by Gonella (1971), results from the observed rotary current at a given depth approaching the inertial frequency. Therefore, energy associated with a diurnal tidal current would not appear as a distinct peak but would be contaminated by energy associated with the inertial current. Further difficulty would be introduced by shifting of frequencies

caused by the presence of mean flow and mass stratification.

Wind-induced inertial oscillations of the surface layer along the Louisiana coast appear to be a fairly common phenomenon if the record examined here is any indication. Because atmospheric fronts are most common and strongest along the Louisiana coast during the winter, early spring, and late fall (Leipper, 1954), these periods can be expected to produce inertial rotary motion frequently. The frequency of frontal passage through the region during this period is one every 3 to 6 days. Thus, inertial currents are probably very commonplace for part of the year. For example, the 32-day winter record examined here contains inertial currents most of the time.

On the other hand, atmospheric fronts decrease in frequency and strength through the late spring, summer, and early fall, when the Bermuda high-pressure system dominates the weather along coastal Louisiana. Therefore, inertial currents are much less likely to be observed during this period. As an example, the 39-day record beginning 25 April and ending 2 June contains only one distinct case of inertial motion.

REFERENCES

Bendat, J. S., and A. G. Piersol, 1966, Measurement and analysis of random data. New York (Wiley), 390 pp.

Bernstein, R. L., 1972, Observations of currents in the Arctic Ocean. Lamont-Doherty Geological Observatory, Palisades, New York, Tech. Rept. 7.

Blackman, R., and J. Tukey, 1959, The measurement of power spectra. New York (Dover), 190 pp.

Bloomfield, P., 1976, Fourier analysis of time series. New York (Wiley), 258 pp.

Brigham, E., 1974, The Fast Fourier Transform. Englewood Cliffs, New Jersey (Prentice-Hall), 252 pp.

Doodson, A. T., and H. D. Warburg, 1941, Admiralty manual of tides. British Admiralty, Hydrographic Dept., 270 pp.

Fofonoff, N. P., 1969, Spectral characteristics of internal waves in the ocean. Deep-Sea Res., 16, supplement, pp. 58-71.

Gonella, J., 1971, A local study of inertial oscillations in the upper layers of the ocean. Deep-Sea Res., 18:775-788.

Gonella, J., 1972, A rotary-component method for analyzing meteorological and oceanographic vector time series. Deep-Sea Res., 19:833-846.

Groves, G. W., 1955, Numerical filters for discrimination against tidal periodicities. Trans. Am. Geophys. Union, 36(6):1073-1084.

Holloway, J. L., 1958, Smoothing and filtering of time series and space fields. Adv. Geophys., 4:351-389.

Hsu, S. A., 1974, On the log-linear wind profile and the relationship between shear stress and stability characteristics over the sea. Boundary-Layer Meteorol., 6:509-514.

Hunkins, K., 1967, Some inertial oscillations of Fletcher's Island (T-3). J. Geophys. Res., 72(4):1164-1174.

Kato, H., and O. Phillips, 1969, On the penetration of a turbulent layer into stratified fluid. J. Fluid Mech., 37:643-655.

Knauss, J. A., 1962, Observations of internal waves of tidal period made with neutrally buoyant floats. J. Mar. Res., 20(2):111-118.

Lathi, B., 1968, An introduction to random signals and communication theory. Scranton, Pennsylvania (International Textbook Co.), 488 pp.

Leipper, D., 1954, Marine meteorology of the Gulf of Mexico: a brief review. Fishery Bull. 89, vol. 55, pp. 89-98.

Marmer, H., 1954, Tides and sea level in the Gulf of Mexico. Fishery Bull. 89, vol. 55, pp. 101-118.

Mooers, C., 1973, A technique for the cross spectrum analysis of pairs of complex-value time series, with emphasis on properties of polarized components and rotational invariants. Deep-Sea Res., 20:1129-1141.

National Ocean Survey, 1974, Tide tables. Dept. of Commerce, Washin ton, D.C.

Neumann, G., 1968, Ocean currents. New York (Elsevier), 352 pp.

Neumann, G., and W. Pierson, 1966, Principles of physical oceanography. Englewood Cliffs, New Jersey (Prentice-Hall).

Perkins, H. T., 1970, Inertial oscillations in the Mediterranean. Ph.D. dissertation, Massachusetts Institute of Technology-Woods Hole Oceanographic Institution, 123 pp.

Perkins, H., 1972, Inertial oscillations in the Mediterranean. Deep-Sea Res., 19:289-296.

Pollard, R. T., 1970, On the generation by winds of inertial waves in the ocean. Deep-Sea Res., 17:795-812.

Pollard, R. T., and R. C. Millard, Jr., 1970, Comparison between observed and simulated wind-generated inertial oscillations. Deep-Sea Res., 17:813-821.

Reid, J. L., 1962, Observations of inertial rotation and internal waves. Deep-Sea Res., 9(4):283-289.

Stommel, H., 1954, Serial observations of drift currents in the central North Atlantic Ocean. Tellus, 6:203-214.

Sverdrup, H. U., M. A. Johnson, and R. H. Fleming, 1942, The oceans. Englewood Cliffs, New Jersey (Prentice-Hall).

Swallow, J. C., 1957, Some further deep current measurements using neutrally-buoyant floats. Deep-Sea Res., 2(2):93-104.

Tukey, J. W., 1961, Discussion emphasizing the connection between analysis of variance and spectrum analysis. Technometrics, 3:191-228.

Webster, F., 1968, Observations of inertial-period motions in the deep sea. Rev. Geophys., 6(4):473-490.

Wiseman, W. J., S. P. Murray, J. M. Bane, and M. W. Tubman, 1976, Offshore physical oceanography. In (J. G. Gosselink, R. R. Miller, M. Hood, and L. M. Bahr, Jr., eds.) Louisiana Offshore Oil Port: environmental baseline study. LOOP, Inc., New Orleans, La.

UNCLASSIFIED DISTRIBUTION LIST
Reports of Contract N00014-75-C-0192, Project NR 388 002

Office of Naval Research
Geography Programs
Code 462
Arlington, Virginia 22217

Defense Documentation Center
Cameron Station
Alexandria, Virginia 22314

Director, Naval Research Lab
Attn: Technical Information Officer
Washington, D.C. 20375

Director
Office of Naval Research Branch Office
219 Dearborn Street
Chicago, Illinois 60604

Director
Office of Naval Research
Branch Office
1030 East Green Street
Pasadena, California 91101

Director
Office of Naval Research
Branch Office
495 Summer Street
Boston, Massachusetts 02210

Commanding Officer
Office of Naval Research
Branch Office
Box 39
FPO New York 09510

Chief of Naval Research
Asst. for Marine Corps Matters
Code 100M
Office of Naval Research
Washington, D.C. 22217

NORDA
Code 400
National Space Technology Lab
Bay St. Louis, MS 39520

Office of Naval Research
Operational Applications Div.
Code 200
Arlington, Virginia 22217

Office of Naval Research
Scientific Liaison Officer
Scripps Inst. of Oceanography
La Jolla, California 92038

Director, Naval Research Lab
Attn. Library, Code 2628
Washington, D.C. 20375

Commander
Naval Oceanographic Office
Attn. Library, Code 1600
Washington, D.C. 20374

Naval Oceanographic Office
Code 3001
Washington, D.C. 20374

Chief of Naval Operations
OP 987P1
Department of the Navy
Washington, D.C. 20350

Oceanographer of the Navy
Hoffman II Building
200 Stovall Street
Alexandria, Virginia 22322

Naval Academy Library
U.S. Naval Academy
Annapolis, Maryland 21402

Commanding Officer
Naval Coastal Systems Laboratory
Panama City, Florida 32401

Librarian
Naval Intelligence
Support Center
4301 Suitland Road
Washington, D.C. 20390

Commanding Officer
Naval Civil Engineering Lab
Port Hueneme, California 93041

Officer in Charge
Environmental Prediction
Research Facility
Naval Post Graduate School
Monterey, California 93940

Dr. Warren C. Thompson
Dept. of Meteorology and
Oceanography
U.S. Naval Post Graduate School
Monterey, California 93940

Director
Amphibious Warfare Board
U.S. Atlantic Fleet
Naval Amphibious Base
Norfolk, Little Creek, Va. 23520

Commander, Amphibious Force
U.S. Pacific Fleet
Force Meteorologist
COMPHIBPAC CODE 25 5
San Diego, California 92155

Commanding General
Marine Corps Development and
Educational Command
Quantico, Virginia 22134

Dr. A. L. Slafkosky
Scientific Advisor
Commandant of the Marine Corps
Code MC-RD-1
Washington, D.C. 20380

Defense Intelligence Agency
Central Reference Division
Code RDS-3
Washington, D.C. 20301

Director
Coastal Engineering Res. Center
U.S. Army Corps of Engineers
Kingman Building
Fort Belvoir, Virginia 22060

Chief, Wave Dynamics Division
USAE-WES
P.O. Box 631
Vicksburg, Miss. 39180

Commandant
U.S. Coast Guard
Attn: GECV/61
Washington, D.C. 20591

Office of Research and
Development
c/o DS/62
U.S. Coast Guard
Washington, D.C. 20591

National Oceanographic
Data Center c/o D764
Environmental Data Services
NOAA
Washington, D.C. 20235

Central Intelligence Agency
Attn: OCR/DD-Publications
Washington, D.C. 20205

Dr. Donald Swift
Marine Geology and
Geophysics Laboratory
AOML - NOAA
15 Rickenbacker Causeway
Miami, Florida 33149

Ministerialdirektor
Dr. F. Wever
Rue/FO
Bundesministerium der
Verteidigung
Hardthoehe
D-5300 Bonn, West Germany

Dr. Yoshimi Goda
Director, Wave Research Div.
Port and Harbor Research Inst.
Ministry of Transportation
I-1 Nagase, 3 Chome
Yokosuka, 239 Japan

Mr. Tage Starup
Defence Research Establishment
Osterbrogades Kaserne
DK-2100 Kobenhavn O, Denmark

Prof. Dr. Rer. Nat. H. G.
Gierloff-Emden
Institut F. Geographie
Universitaet Muenchen
Luisenstrasse 37/111
D-800 Muenchen 2, West Germany

Prof. Dr. Eugen Seibold
Geol-Palaeontolog. Institut
Universitaet Kiel
Olshausenstrasse 40-60
D-2300 Kiel, West Germany

Dr. R. Koester
Geo.-Palaeontolog. Institut
Universitaet Kiel
Olshausenstrasse 40-60
D-2300 Kiel, West Germany

Prof. Dr. Fuehrboeter
Lehrstuhl F. Hydromechanik U.
Kuestenwasserbau
Technische Hochschule
Braunschweig
Beethovenstrasse 51A
D-3300 Braunschweig
West Germany

Prof. Dr. Walter Hansen
Direktor D. Instituts f.
Meereskunde
Universitaet Hamburg
Heimhuderstrasse 71
D-2000 Hamburg 13,
West Germany

Prof. Dr. Klaus Hasselmann
Institut F. Geophysik
Universitaet Hamburg
Schleuterstrasse 22
D-2000 Hamburg 13,
West Germany

Prof. Dr. Nils Jerlov
Institute for Physical
Oceanography
Kobenhavns Universitet
Haraldsgade 6
DK-2200 Kobenhavn, Denmark

Dr. Vernon W. Pidgeon
Dynex Consulting Company
1001 Kimberly Lane
Lynn Haven, Florida 32444

Ir. H. J. Schoemaker
Waterloopkundig Laboratorium
Te Delft
61 Raam, Delft, Netherlands

Ir. M. W. Van Batenberg
Physisch Laboratorium TNO
Oude Waalsdorper Weg 63,
Den Haag
Netherlands

Mr. H. G. Tornatore
ITT Avionics
9140 Old Annapolis Road
Columbia, Maryland 21043

ONR Scientific Liaison Group
American Embassy
Room A-407
APO San Francisco 96503

Coastal Studies Institute
Louisiana State University
Baton Rouge, Louisiana 70803

Dr. Bernard Le Mehaute
Tetra Tech, Inc.
630 North Rosemead Blvd.
Pasadena, California 91107

Dr. Richard A. Davis, Jr.
Department of Geology
University of South Florida
Tampa, Florida 33620

Dr. William T. Fox
Department of Geology
Williams College
Williamstown, Mass. 01267

Dr. William S. Gaither
Dean
College of Marine Studies
Robinson Hall
University of Delaware
Newark, Delaware 19711

Dr. John T. Kuo
Henry Krumb School of Mines
Seeley W. Mudd Building
Columbia University
New York, New York 10027

Dr. Edward B. Thornton
Department of Oceanography
Naval Postgraduate School
Monterey, California 93940

Prof. C. A. M. King
Department of Geography
University of Nottingham
Nottingham, England

Dr. Douglas L. Inman
Scripps Institute of
Oceanography
La Jolla, California 92037

Prof. Toshiyuki Shigemura
Civil Engineering Dept.
National Defense Academy
1-10-20 Hashirimizu
Yokosuka 239, Japan

Prof. Yuji Iwagaki
Civil Engineering Dept.
Kyoto University
9 Shimogamo Zenbucho, Sakyo-Ku
Kyoto, Japan

Prof. Kiyoshi Horikawa
Dept. of Civil Engineering
University of Tokyo
7-3-1, Hongo, Bunkyo-Ku
Tokyo 113, Japan

Dr. William W. Wood
Department of Geosciences
Purdue University
Lafayette, Indiana 47907

Dr. Alan W. Niedoroda
Director, Coastal Research
Center
University of Massachusetts
Amherst, Mass. 01002

Dr. Benno M. Brenninkmeyer,
S.J.
Dept. of Geology & Geophysics
Boston College
Chestnut Hill, Mass. 02167

Dr. Omar Shemdin
JPL-CALTECH
Mail Stop 183-501
4800 Oak Grove Drive
Pasadena, California 91103

Dr. Lester A. Gerhardt
Rennsselaer Polytechnic Inst.
Troy, New York 12181

Mr. Fred Thomson
Environmental Research Inst.
P.O. Box 618
Ann Arbor, Michigan 48107

Dr. J. A. Dracup
Environmental Dynamics, Inc.
1609 Westwood Blvd.
Suite 202
Los Angeles, Calif. 90024

Dr. Thomas K. Peucker
Simon Fraser University
Department of Geography
Burnaby 2, B.C., Canada

Dr. Bruce Hayden
Department of Environmental
Sciences
University of Virginia
Charlottesville, VA 22903

Revised 1/11/77

Unclassified
Security Classification

DOCUMENT CONTROL DATA - R & D

(Security classification of title, body of abstract and indexing annotation must be entered when the overall report is classified)

1. ORIGINATING ACTIVITY (Corporate author)
Coastal Studies Institute
Louisiana State University
Baton Rouge, Louisiana 70803

2a. REPORT SECURITY CLASSIFICATION
Unclassified

2b. GROUP
Unclassified

3. REPORT TITLE
RESPONSE OF COASTAL WATERS TO ATMOSPHERIC FRONTAL PASSAGE IN THE MISSISSIPPI DELTA REGION

4. DESCRIPTIVE NOTES (Type of report and inclusive dates)

5. AUTHOR(S) (First name, middle initial, last name)
Ernest Daddio

6. REPORT DATE	7a. TOTAL NO. OF PAGES	7b. NO. OF REFS
May 1977	35	33

8a. CONTRACT OR GRANT NO.	9a. ORIGINATOR'S REPORT NUMBER(S)
N00014-75-C-0192	Technical Report No. 234
b. PROJECT NO NR 388 002	9b. OTHER REPORT NO(S) (Any other numbers that may be assigned this report)
c.	
d.	

086 700

10. DISTRIBUTION STATEMENT
Approved for public release; distribution unlimited.

11. SUPPLEMENTARY NOTES	12. SPONSORING MILITARY ACTIVITY
	Geography Programs Office of Naval Research Arlington, Virginia 22217

13. ABSTRACT

Two current vector time series obtained in the Mississippi Bight exhibit clockwise polarized currents of near-inertial frequency that are closely associated with shifting winds. Because of the closeness of the local inertial period and the diurnal tidal period, it is difficult at first glance to determine the true nature of the observed rotary currents. However, complex demodulation at the inertial frequency reveals a strong signal accompanying wind shifts that are usually associated with the passage of atmospheric fronts. (U)

Spectral analysis for clockwise and counterclockwise frequencies indicates a highly energetic peak in the inertial-diurnal frequency band for the clockwise spectrum. The rotary coefficient computed from the autospectra and quadrature spectrum of the vector components gives $C_R > 0.9$ in the vicinity of the inertial-diurnal frequency band. (U)

A model using wind stress as a forcing function is highly effective in reproducing sinusoidal oscillations seen in the observed current. These oscillations occur in conjunction with shifts in the wind direction. (U)

Because of the close association of the near-inertial oscillations with local wind effects, it is concluded that inertial currents are locally induced by wind stress. Furthermore, wind stress not only initiates the rotary currents but is also highly effective in destroying them. (U)

DD FORM 1 NOV 65 1473 (PAGE 1)
S/N 0101-807-6811

Unclassified
Security Classification

A-31408

14 KEY WORDS	LINK A		LINK B		LINK C	
	ROLE	WT	ROLE	WT	ROLE	WT
Currents						
Mississippi Bight						
Inertial frequency						
Wind stress						
Sinusoidal oscillations						